

1     **Radar interferometry techniques for the study of ground subsidence**  
2     **phenomena: a review of practical issues through cases in Spain**

3  
4     Tomás, R.<sup>1,2</sup>, Romero, R.<sup>3</sup>, Mulas, J.<sup>2,4</sup>, Marturià, J.J.<sup>5</sup>, Mallorquí, J.J.<sup>6</sup>, Lopez-Sanchez,  
5     J.M.<sup>2,7</sup>, Herrera, G.<sup>2,4</sup>, Gutiérrez, F.<sup>8</sup>, González, P.J.<sup>9</sup>, Fernández, J.<sup>10</sup>, Duque S.<sup>6</sup>,  
6     Concha-Dimas, A.<sup>5</sup>, Cocksley, G.<sup>11</sup>, Castañeda, C.<sup>12</sup>, Carrasco, D.<sup>3</sup>, Blanco, P.<sup>13</sup>

7  
8     (1) Departamento de Ingeniería de la Construcción, Obras Públicas e Infraestructura  
9     Urbana, Escuela Politécnica Superior, Universidad de Alicante, P.O. Box 99, E-  
10     03080 Alicante, Spain. Tel. (+34) 965903400. [Roberto.tomas@ua.es](mailto:Roberto.tomas@ua.es)

11    (2) Unidad Asociada de investigación IGME-UA de movimientos del terreno mediante  
12    interferometría radar (UNIRAD).

13    (3) INDRA Espacio, Mar Egeo 4, Pol. Industrial nº 1, San Fernando de Henares,  
14    Madrid, 28830, Spain. Tel. (+34) 914805000. [rromero@indra.es](mailto:rromero@indra.es)

15    (4) Geohazards Remote Sensing Laboratory, Grupo de Riesgos Geológicos, Instituto  
16    Geológico y Minero de España, Ríos Rosas 23, E-28003 Madrid, Spain. Tel. (+34)  
17    91349 5785. [j.mulas@igme.es](mailto:j.mulas@igme.es), [g.herrera@igme.es](mailto:g.herrera@igme.es)

18    (5) Institut Geològic de Catalunya, Balmes 209-211, Barcelona, Spain. Tel. (+34)  
19    935538430. [jmarturia@igc.cat](mailto:jmarturia@igc.cat)

20    (6) Remote Sensing Lab., Departament de Teoria del Senyal I Comunicacions,  
21    Universitat Politècnica de Catalunya, Campus Nord Ed. D3, Jordi Girona 1-3,  
22    08034 Barcelona, Spain. Tel. (+34) 934017229. [mallorqui@tsc.upc.edu](mailto:mallorqui@tsc.upc.edu)

23    (7) Departamento de Física, Ingeniería de Sistemas y Teoría de la Señal (DFISTS),  
24    Escuela Politécnica Superior, Universidad de Alicante, P.O. Box 99, E-03080  
25    Alicante, Spain. Tel. (+34) 965909597. [Juanma.lopez@ua.es](mailto:Juanma.lopez@ua.es)

- 26 (8) Department of Earth Sciences, University of Zaragoza. Pedro Cerbuna 12, 50009  
27 Zaragoza, Spain. Tel. (+34) 976761090. [fgutier@unizar.es](mailto:fgutier@unizar.es)
- 28 (9) Department of Earth Sciences, University of Western Ontario, Biological &  
29 Geological Sciences Building, London, Ontario, N6A 5B7, Canada.  
30 [pgonzal4@uwo.ca](mailto:pgonzal4@uwo.ca)
- 31 (10) Institute of Geosciences (CSIC-UCM), Facultad de Ciencias Matemáticas, Plaza de  
32 Ciencias 3, 28040 Madrid, Spain. Tel. (+34) 913944632. [jft@mat.ucm.es](mailto:jft@mat.ucm.es)
- 33 (11) Altamira Information, Còrsega 381-387, E-08037 Barcelona, Spain. Tel. (+34)  
34 931835750. [geraint.cooksley@altamira-information.com](mailto:geraint.cooksley@altamira-information.com)
- 35 (12) Estación Experimental de Aula Dei (EEAD-CSIC), P.O. Box 13034, 50080  
36 Zaragoza, Spain. Tel. (+34) 976716069. [ccastaneda@eead.csic.es](mailto:ccastaneda@eead.csic.es)
- 37 (13) Institut Cartografic de Catalunya, Balmes 209-211, Barcelona, Spain. Tel. (+34)  
38 935671500. [pablo.blanco@icc.cat](mailto:pablo.blanco@icc.cat)

39

#### 40 Abstract

41 Subsidence related to multiple natural and human-induced processes affects an  
42 increasing number of areas worldwide. Although this phenomenon may involve surface  
43 deformation with 3D displacement components, negative vertical movement, either  
44 progressive or episodic, tends to dominate. Over the last decades, Differential SAR  
45 Interferometry (DInSAR) has become a very useful remote sensing tool for accurately  
46 measuring the spatial and temporal evolution of surface displacements over broad areas.  
47 This work discusses the main advantages and limitations of addressing active  
48 subsidence phenomena by means of DInSAR techniques from an end-user point of  
49 view. Special attention is paid to the spatial and temporal resolution, the precision of the  
50 measurements, and the usefulness of the data. The presented analysis is focused on

51 DInSAR results exploitation of various ground subsidence phenomena (groundwater  
52 withdrawal, soil compaction, mining subsidence, evaporite dissolution subsidence and  
53 volcanic deformation) with different displacement patterns in a selection of subsidence  
54 areas in Spain. Finally, a cost comparative study is performed for the different  
55 techniques applied.

56

57 Keywords: subsidence, DInSAR, settlement, remote sensing, Spain, technique-cost

58

## 59 1. Introduction

60 The term subsidence refers to the sudden sinking or gradual downward settling of the  
61 ground surface with little or no horizontal motion (Jackson 1997). Active subsidence  
62 may be related to multiple natural and anthropogenic processes (Corapcioglu 1989;  
63 Waltham 1989; Galloway et al. 1999). The risk to people and their infrastructures posed  
64 by subsidence phenomena in remote and non-inhabited areas is generally negligible.  
65 However, active subsidence in developed areas may cause significant damage to human  
66 structures, often involving multi-million dollar losses (e.g. Kappel et al. 1999; Autin  
67 2002; Gutiérrez et al. 2009; Mancini et al. 2009). Wu (2003) points out that subsidence  
68 constitutes a hazard for bridges, roads, railways, storm drains, sewers, canals, levees,  
69 buildings and well pipes, and increases the susceptibility to tidal flooding in low-lying  
70 coastal areas. Moreover, catastrophic subsidence may result in human life lost (Guerrero  
71 et al. 2008; Galve et al. 2012). For instance, in the Far West Rand of South Africa,  
72 sudden sinkholes induced by dewatering of dolomite aquifers for gold mining have  
73 caused a total of 38 fatalities (De Bruyn and Bell 2001).

74 Land subsidence is the surface evidence of shallow or deep-seated deformation induced  
75 by a wide variety of natural or anthropogenic subsurface processes. Following

76 Prokopovich's genetic classification of subsidence (1979), endogenic subsidence is  
77 associated with internal geological processes such as faulting, folding, isostatic  
78 adjustments and volcanism. Exogenic subsidence is related to anthropogenic or natural  
79 processes involving the creation of cavities and/or the removal of material from the  
80 subsurface. The main causal mechanisms of exogenic subsidence include dissolution,  
81 degradation of organic matter, piping, thawing of ground ice, bioturbation, piezometric  
82 falls related to reduced aquifer recharge, fluid withdrawal (e.g. water, petroleum and  
83 gas), underground mining, tunnelling (Waltham 1989; Galloway et al. 1999; Gonzalez  
84 de Vallejo and Ferrer 2011).

85 In the pre-mitigation investigation phase, a combination of scientific understanding of  
86 these processes and a careful management can minimize the subsidence. Then,  
87 subsidence investigations are important to delineate the extent of the affected area,  
88 measuring the surface displacements (magnitude, rate and temporal and spatial  
89 variability), determining the strain mechanisms and identifying precursory/premonitory  
90 displacement indicative of potential catastrophic subsidence events in order to propose  
91 and design mitigation measures. Once mitigation measures are applied, subsidence  
92 monitoring allows evaluating the effectiveness of the adopted corrective or preventative  
93 measures, and forecasting the future behaviour of the subsidence phenomena. Numerous  
94 techniques are used for measuring and mapping spatial gradients and temporal rates of  
95 regional and local subsidence (Galloway et al. 1998; Galloway and Burbey 2011). The  
96 approaching selection is generally based on several key factors (Tomás et al. 2008;  
97 Galloway and Burbey 2011) including:

- 98 1) the cost, usually the most relevant conditioning parameter;
- 99 2) the required accuracy and resolution, conditioned by the type of subsidence  
100 phenomenon;

- 101 3) the type of data (punctual, linear, spatially distributed) and measuring frequency
- 102 (time between measurement acquisitions), which are largely determined by the
- 103 subsidence pattern (extent, rate, spatial and temporal variability);
- 104 4) land cover (rock outcrops, forest, urban, etc.), and weather conditions;
- 105 5) flexibility of the method, related to the possibility to selecting the time and location
- 106 of the measurement acquisition, the data availability (ease of access to the data), as well
- 107 as the acquisition time (time required to complete a measurement campaign); and
- 108 6) geometry and the kinematics of the subsidence phenomenon.

109 This paper reviews DInSAR data exploitation related to different ground subsidence  
110 phenomena (groundwater withdrawal, soil compaction, mining and evaporite  
111 dissolution subsidence and volcanic deformation) investigated in nineteen areas of  
112 Spain (Figure 1). Targeted subsidence areas differ in their extent, subsidence rates, and  
113 temporal evolution. This work highlights the main advantages and limitations of  
114 addressing the investigation of active subsidence with DInSAR techniques from an end-  
115 user point of view; i.e. spatial and temporal resolution, precision of the measurements,  
116 and utility of the data. Finally, a discussion on the cost-effectiveness of the different  
117 monitoring techniques used in Spain is presented.

118

119 Figure 1. Subsidence areas investigated by means of the Differential SAR  
120 Interferometry (DInSAR) technique in Spain and reported in this work.

121

122 2. A brief introduction to DInSAR

123 Synthetic Aperture Radar (SAR) and its derived techniques, like SAR interferometry  
124 (InSAR), have been widely addressed and reviewed in the scientific literature  
125 (Massonnet and Feigl 1998; Bamler and Hartl 1998; Ferretti et al. 2001; Hanssen 2001;

126 Crosetto et al. 2005b; Kampes 2006; Simons and Rosen 2007; Prati et al. 2010; Hooper  
127 et al. 2012). One of the main applications of SAR interferometry is the detection of  
128 Earth's surface displacements through Differential Interferometry (DInSAR), which has  
129 shown to be a tool of great potential over the last decades. Initial single interferogram  
130 DInSAR techniques, commonly referred to as conventional DInSAR techniques,  
131 (Massonnet et al. 1993; Peltzer and Rosen 1995) evolved to advanced DInSAR  
132 techniques which provide information on the temporal evolution of the ground  
133 displacement, with a theoretical millimetric precision under favourable conditions.  
134 According to Sansosti et al. (2010), advanced DInSAR techniques can be grouped into  
135 two main categories: Persistent Scatterers (PS) methods that work on localized targets  
136 (Ferretti et al. 2001; Arnaud et al. 2003; Werner et al. 2003), and Small Baseline (SB)  
137 methods that utilize spatially distributed targets (Lundgren et al. 2001; Berardino et al.  
138 2002; Mora et al. 2003; Schmidt and Bürgmann 2003; Prati et al. 2010). Such  
139 techniques have been applied to ground displacements related to active tectonics,  
140 seismic events, volcanism, anthropogenic subsidence and uplift, landsliding or glacier  
141 dynamics.

142 The basic concept of the DInSAR techniques is to monitor an area through time on a  
143 regular basis. The SAR images acquired in different dates are then combined in pairs to  
144 generate a set of differential interferograms that contain information on the  
145 interferometric phase ( $\psi_{\text{int}}$ ). Ideally, differential interferograms should contain only the  
146 ground displacement component between the acquisition times of the two SAR images.  
147 However, in practice, there are other terms contributing to the interferometric phase that  
148 can mask the desired ground displacement information, e.g. phase contributions from  
149 atmospheric water vapour ( $\psi_{\text{atmos}}$ ). The goal of the different processing techniques is to  
150 accurately isolating the displacement term from the remaining components. The

151 interferometric phase can be expressed as the sum of the following terms (Hanssen  
152 2001):

$$153 \quad \psi_{\text{int}} = \psi_{\text{flat}} + \psi_{\text{topo}} + \psi_{\text{mov}} + \psi_{\text{atmos}} + \psi_{\text{noise}} \quad (1)$$

154 where  $\psi_{\text{flat}}$  is the flat-earth component related to range distance differences in absence  
155 of topography,  $\psi_{\text{topo}}$  is the topographic phase,  $\psi_{\text{mov}}$  is the phase contribution due to  
156 ground displacement occurring between the two SAR image acquisitions, measured  
157 along the line of sight (LOS),  $\psi_{\text{atmos}}$  is the phase component due to atmospheric  
158 disturbances or artefacts, and  $\psi_{\text{noise}}$  includes the remaining noise sources. The first two  
159 terms in (1) can be expressed analytically and  $\psi_{\text{topo}}$  can be extracted from an  
160 independent DEM.

161 The degradation of the quality of the interferometric phase (decorrelation) has a non-  
162 uniform impact on the interferograms. Depending on several factors like the land cover,  
163 presence of human structures, surface changes due to human or natural activity, some  
164 areas may have a better quality phase. Consequently, a selection of the more reliable  
165 pixels from a set of interferograms has to be performed. The pixel selection criterion  
166 can be established based on the estimation of their phase quality using two different  
167 approaches: the *coherence stability* and the *amplitude dispersion*. For the former, a  
168 multi-looked pixel is selected if it presents coherence values higher than an established  
169 threshold in a certain percentage of interferograms (Berardino et al. 2002; Mora et al.  
170 2003). For the latter, the phase standard deviation of each pixel is assumed to be related  
171 to its temporal radar signal amplitude stability (low dispersion) and selected if it  
172 exceeds a certain threshold (Ferretti et al. 2001). The selection criterion determines the  
173 nature of the targets to work with. While the amplitude dispersion selects ideal point-  
174 like targets at the maximum spatial resolution of the SAR image, the coherence stability  
175 implies an averaging of a set of pixels, leading to a lower spatial resolution product.

176 Depending on the setting, it may be necessary to decrease the number of selected points  
177 by employing a coherence approach, rather than having the maximum spatial resolution  
178 information provided by the amplitude approach. For instance, in volcanic areas where  
179 rock outcrops have large extent and temporal stability, the coherence-based processing  
180 is generally more appropriate. In contrast, in urban areas where man-made targets are  
181 more likely to be found, the amplitude-based processing is typically better suited.  
182 Another decisive issue is the number of available images. A reliable relationship  
183 between amplitude and phase stability cannot be obtained with a limited number of  
184 images. On the other hand, the coherence estimator is more robust when dealing with a  
185 low number of interferograms. Considering both criteria, a compromise between the  
186 number of pixels selected and their reliability should be found.

187 For measuring ground displacement, satellite-based DInSAR techniques present three  
188 immediate advantages compared to classical ground-based methods such as the  
189 Differential Global Positioning System (DGPS): low-cost, measurement repetitiveness  
190 and availability of historical data. Firstly, they provide, at a low cost, displacement  
191 measurements across wide areas and with a high spatial density, as opposed to the  
192 discrete point data supplied by instrumental techniques, restricted to benchmarks with a  
193 much lower density and generally covering smaller areas. For instance, the widely used  
194 SAR images acquired by the European ERS or ENVISAT and the German TerraSAR-X  
195 satellites cover an area of 100 km by 100 km and 30 km by 50 km respectively.  
196 Secondly, orbital sensors have a short revisiting time period, which makes it possible to  
197 monitor at selected locations with a high frequency. Thirdly, the low incidence angle  
198 (i.e. the angle between the satellite line-of-sight (LOS) and a line perpendicular to the  
199 land surface) makes InSAR technique very sensitive to vertical displacements produced  
200 by subsidence. Finally, the relatively long archive of SAR images acquired since 1992



201 allows studying, at least in Europe, almost any area since that date. Nevertheless,  
202 DInSAR techniques should be considered as complementary, rather than a complete  
203 replacement of the ground-based techniques.

204

### 205 3. Advantages and limitations of DInSAR from the end-user point of view

206 In the last 20 years the importance of DInSAR as a subsidence monitoring tool has  
207 increased significantly. In Spain, nineteen areas affected by active subsidence have been  
208 studied using different DInSAR techniques. These studies exploit radar data from seven  
209 sensors, which include satellite- and ground-based (Tables 1 and 2). These case studies  
210 deal with subsidence due to groundwater withdrawal, mining activity, volcanism,  
211 impoundment of water reservoir, evaporite dissolution, and the superposition of some of  
212 the above mentioned processes. Although most of these subsidence cases were  
213 previously known and characterized, the application of DInSAR techniques allowed  
214 gaining greater insight into the deformation patterns, specially providing quantitative  
215 strain data. In this section, the main advantages and limitations of the DInSAR  
216 techniques from an end-user point of view are discussed and illustrated through  
217 subsidence case studies from Spain.

218

219 Table 1. Radar systems employed in the reported subsidence studies in Spain. ESA:  
220 European Space Agency; DLR: German Aerospace Center; JAXA: Japan Aerospace  
221 Exploration Agency; UPC: Universidad Polit cnica de Catalu a; ASI: Italian Space  
222 Agency.

223

224 Table 2. DInSAR technique and pixel selection criteria implemented in the software  
225 packages applied to study subsidence in Spain. Software developer is also indicated.

226

### 227 3.1 Spatial resolution

228 The spatial resolution of DInSAR data is crucial in subsidence studies with an applied  
229 objective. The spatial resolution of the ground displacement data depends on the radar  
230 sensor and the processing algorithm. The pixel selection methods based on amplitude  
231 criteria allow keeping the original resolution of the SAR image. On the other hand, by  
232 definition, coherence selection techniques involve an averaging of adjacent pixels of the  
233 original image with the consequent degradation in spatial resolution. Using the  
234 coherence approach, typical resolutions of DInSAR maps obtained from ERS and  
235 ENVISAT data are  $60\text{ m} \times 60\text{ m}$ ,  $80\text{ m} \times 80\text{ m}$  and  $100\text{ m} \times 100\text{ m}$ . These values  
236 correspond to the multilook averaging of  $3 \times 15$ ,  $4 \times 20$ , and  $5 \times 25$  pixels in azimuth  
237 and range respectively. Spatially restricted subsidence phenomena, such as those related  
238 to evaporite dissolution-induced sinkholes in the *Ebro Valley* (Castañeda et al. 2009b)  
239 or a salt mine below *Sallent* village (López et al. 2010), usually affect areas smaller than  
240  $1\text{ km}^2$ . Consequently, they require an appropriate compromise between resolution and  
241 electromagnetic response stability. As an example, the 80-m pixel-sized DInSAR map  
242 of Figure 2 provides partial displacement data on a subsidence basin induced by  
243 underground mining but does not allow analysing subsidence at a building scale  
244 (Herrera et al. 2012). DInSAR applications for built areas and infrastructures require  
245 very high resolutions in order to obtain information on individual buildings or elements  
246 of a structure rather than an averaged subsidence rate for an area including several  
247 constructions. For *Murcia* city (Figure 3), Herrera et al. (2009b) demonstrated that  
248 amplitude techniques, which work at full resolution, provide a higher density of reliable  
249 points than coherence based techniques. Moreover, using different bands TSX has  
250 demonstrated to provide the highest PSs density (Crosetto et al. 2010; Herrera et al.

251 2010). Figure 3 shows that the X-band based PSs density is at least ten times higher  
252 than the PSs density provided by C-band satellites (Herrera et al. 2010).

253

254 Figure 2. Detail of the 80-m pixel-sized DInSAR map of mining subsidence in La  
255 Unión for the period 2005-2008. Grey line corresponds to the 1:5000 topographic map.

256

257 Figure 3. DInSAR maps showing subsidence rates caused by aquifer overexploitation in  
258 the *Vega Media of the Segura River* (Spain) obtained from images acquired by different  
259 sensors and for three successive of time periods: a) 1995-2005 period (ERS and  
260 ENVISAT sensors). b) 2005-2008 period (ENVISAT sensor). c) 2008-2009 period  
261 (TerraSAR-X sensor). d) Temporal evolution of the subsidence from 1995 to 2009,  
262 plotted alongside the variations in the piezometric level.  $Syr^{-1}$  is the average number of  
263 SAR images per year, and  $dgp$  is the existing maximum temporal gap (expressed in  
264 days) between two SAR images.

265

### 266 3.2 Temporal resolution

267 The temporal resolution of the ground displacement data depends on the satellite  
268 revisiting period (Table 1) that determines the availability of SAR images of the study  
269 area. Consequently, generally the shorter the revisiting time the more accurate may be  
270 the analysis of the temporal evolution of the subsidence phenomenon. In areas with high  
271 subsidence rates the revisiting period should be as short as possible in order to avoid  
272 aliasing problems. Aliasing is introduced when the sampling frequency is too low and  
273 affects the motion of ground targets or pixels with LOS displacement between the two  
274 dates under study is greater than the system resolution; i.e. half the radar wavelength  
275 ( $\lambda/2$ ). Moreover, shorter revisiting periods improve the ability to identify non-linear or

276 seasonal displacement patterns. COSMO SkyMed and TerraSAR-X, with the shortest  
277 revisiting periods (Table 1), are more appropriate systems to study non-linear and  
278 episodic subsidence phenomena than e.g. ALOS-PALSAR with longer revisiting  
279 periods, although they are more prone to temporal decorrelation in non-urban areas due  
280 to their sensitivity of phase values to any change in scatterers distribution (Prati et al.  
281 2010). As an example, *La Unión* area (Figure 4) exhibits significant gaps of  
282 displacement information due to high deformation rates (4.8 cm per month) related to  
283 mining subsidence (Herrera et al. 2007).

284 The acquisition time of terrestrial sensors (Ground based SAR- GBSAR), which is  
285 selected by the user, allows to define the time between successive acquisitions as much  
286 as few minutes. However, although radar sensors can be strategically placed in  
287 prominent locations in order to get an optimal LOS they are generally limited by the  
288 high incidence angle (Pipia et al. 2007; 2008; Monserrat 2012). ERS and ENVISAT  
289 satellites provide a long historical archive of radar data for almost all the Spanish  
290 territory between 1992 and 2012 with a gap during 1994, allowing to retrospectively  
291 processing data in areas where ground-based data is lacking. Historical data are  
292 necessary for the long-term monitoring of areas with low subsidence rate and for the  
293 application of advanced DInSAR techniques which require a large number of images. In  
294 contrast, TerraSAR-X data is limited to the areas where acquisitions have been  
295 previously requested; i.e. on-demand system. The same applies to GB-SAR, since also  
296 data availability is limited to planned images in monitored areas.

297 Another important issue for DInSAR subsidence analysis is the sensor wavelength ( $\lambda$ ).  
298 Most studies reviewed in this work are based on C-band sensors due to high data  
299 availability. However, DInSAR based on C-band radar data is frequently limited due to  
300 the incoherence/decorrelation related to the land covers. In this sense, in *Sant Quirte del*

301 *Valles* (see location in Figure 1), Blanco et al. (2008) observed that L band-based  
302 DInSAR ( $\lambda = 23$  cm) provides coherent information where C band-based DInSAR ( $\lambda =$   
303 5.6 cm) measurements are predominantly incoherent showing that a significant part of  
304 the backscattered echo arrives from the ground rather than from vegetation in agreement  
305 with other authors (Colesanti and Wasowski 2006; e.g. Raucoules et al. 2007; Hooper et  
306 al. 2012) .

307

308 Figure 4. Detail of C-band DInSAR map of *La Unión*, showing the effect of aliasing on  
309 the availability of Persistent Scatterers due to ~~for~~ high subsidence rates related to  
310 mining. The lack of colored pixels (displacement data) in the urban area of *Lo Tacón* is  
311 due to the loss of coherence. Levelling isolines indicates cumulative displacement in cm  
312 during the time period 1998-2000 and show a displacement rates higher than 40  
313 mm/year (Rodríguez-Estrella et al. 2000).

314

### 315 3.3 Influence of the terrain characteristics on persistent scatterers detection

316 The backscattering of the microwave signals depends on the characteristics of the  
317 terrain and the weather conditions at the acquisition time. Generally, vegetated areas  
318 and water bodies disperse the radar emitted SAR signals, reducing the amount of  
319 returned signal to the satellite (Ulaby et al. 1982; Henderson and Lewis 1998). In some  
320 areas the changes in the vegetation between two radar acquisitions can produce such a  
321 significant loss of coherence that the displacement information is almost impossible to  
322 obtain. On the contrary urban areas, or rock outcrops provide a stable electromagnetic  
323 response through time, being considered more suitable for applying DInSAR  
324 techniques. This circumstance is illustrated by studies carried out in the subsidence  
325 areas of Orihuela village (Tomás et al. 2007; 2010b), where PS densities from 0 to 10

326 PS per km<sup>2</sup> have been obtained in rural areas, whereas more than 100 PS per km<sup>2</sup> were  
327 obtained in urbanized areas and zones dominated by rock outcrops (Figure 5). Rocky  
328 areas like the *Tenerife* Island and urban scenarios such as *Murcia* city, *Orihuela* village  
329 or *Sallent* village provide a high amount of PS points. However, the proportion of PS  
330 points is reduced considerably in the agricultural areas of *Vega Media and Baja of the*  
331 *Segura River* (Herrera et al. 2009b; Tomás et al. 2010b), *Granada* basin (Fernandez et  
332 al. 2009; Sousa et al. 2010) and the *Ebro* valley (Castañeda et al. 2009b) (see Figure 1  
333 for locations).

334 The weather conditions also affect the transmission of the microwaves producing  
335 atmospheric artefacts which may limit the use of DInSAR techniques. Variations in  
336 water vapour, temperature, and pressure along the distance travelled by the signal within  
337 the atmosphere can produce a delay in the transmission of the microwaves affecting the  
338 interferometric phase and distorting the phase related to the actual ground displacement.  
339 This fact has been observed in the *Ebro* valley (Figure 6), where a significant proportion  
340 of the interferograms was affected by atmospheric artefacts (Castañeda et al. 2011).

341

342 Figure 5. Detail of DInSAR map based on the Coherent Pixel Technique (CPT)  
343 showing the water withdrawal induced subsidence measured along the LOS in the city  
344 of *Orihuela* and surrounding areas from 1993 to 2009. Note the high and a low density  
345 of PSs in the urban/rocky and agricultural areas, respectively. The lack of PSs in the SE  
346 slope of the mountain is related to its non-favorable orientation with respect to that of  
347 the LOS.

348

349 Figure 6. a) Location of three areas ~~areas~~ affected by active ground deformation in the  
350 *Ebro* Valley analysed using conventional (interferograms) and SBAS techniques. b)

351 Mixed urban-agricultural area with active sinkholes related to evaporite dissolution in a  
352 mantled karst setting. c) Mixed agricultural and natural vegetated area showing active  
353 landslides in a gypsum escarpment affected by river undercutting. d) Area with natural  
354 xerophytic vegetation showing subsidence induced by salt room and pillar mining. On  
355 the numbers on the left images, indicate subsidence rates measured using SBAS. In the  
356 central images, every color fringe corresponds to a  $2\pi$  phase change (2.6 cm). The plots  
357 show displacement time series for selected points (highlighted in green) from 1995 to  
358 2000.

359

### 360 3.4 Type of results

361 Generally, DInSAR provides a great deal of information on subsidence distribution,  
362 magnitude and kinematics, as well as on the processing quality. These data, measured  
363 along satellite LOS, are generally represented as maps that show the displacement  
364 spatial distribution, either average rate or accumulated magnitude. The former  
365 corresponds to the average displacement rate for the considered period of time,  
366 expressed in mm/year or cm/year (e.g. Figure 4), whereas the latter is the total amount  
367 of subsidence with respect to the first SAR acquisition, usually expressed in mm or cm  
368 (e.g. Figures 2 and 4). When conventional interferometry is used, the results can be also  
369 depicted using fringes that represent a  $2\pi$  phase change (Figure 6), which corresponds to  
370 a displacement of  $\lambda/4\pi$  meters, where  $\lambda$  is the wavelength (in meters) of the microwave  
371 used by satellite. Note that ALOS-PALSAR satellite (L-band) has a wavelength of 23.6  
372 cm whilst TerraSAR-X or Cosmo-Skymed-1 satellites (X-band) have a wavelength of  
373 3.1 cm (Table 1). As a consequence, it can be stated that L-band satellite is less  
374 sensitive to the displacement (one fringe corresponds to 11.8 cm instead of the 1.6 cm  
375 of X-band satellites).

376 The temporal evolution of subsidence for a given point can be represented when a set of  
377 images is used in the processing. Therefore, for every radar measurement we provide:  
378 (1) the position of the PS: three geographical coordinates and (2) the temporal evolution  
379 of the displacement over the processed/analysed time period (e.g. Figure 3d).

380

381

### 382 3.5 Applications of DInSAR information

383 A close cooperation between DInSAR specialists and end-users (geoscientists, civil  
384 engineers, land-use planners, Civil Protection Authorities, insurance companies, etc.) is  
385 necessary in order to fully exploit the high capability and practicality of these remote  
386 sensing techniques. In *Spain*, DInSAR has been used for the monitoring of known  
387 subsiding areas, providing spatially denser displacement information of the area of  
388 interest than ground-based techniques. However, one of the most interesting  
389 applications of these interferometric techniques is the early detection of unknown  
390 ground motion (e.g. Crosetto et al. 2005a; Mora et al. 2007; Castañeda et al. 2009a;  
391 Castañeda et al. 2009b; Fernandez et al. 2009; González et al. 2010; González and  
392 Fernández 2011a; Pulido-Bosch et al. 2011). Some Spanish institutions, such as the  
393 Institut Geologic de Catalunya, IGC, (Mora et al. 2007) have periodically and  
394 systematically monitored wide geographical areas in order to recognize areas affected  
395 by subsidence or other ground instability processes in *Catalonia*. The *Geological*  
396 *Hazard Prevention Map of Catalonia* (MPRGC 1:25000) includes the DInSAR  
397 information. This open-accesses cartographic database allows the public to consult, via  
398 the IGC, ground displacement results (Oller et al. 2011).

399 Another interesting application of DInSAR in Spain is the incorporation of ground  
400 displacement data in the development of susceptibility and risk maps. In *Sallent* village,



401 severely affected by subsidence due to salt mining, DInSAR data has been integrated  
402 into a Geographical Information System (GIS) together with abundant spatial data  
403 (geological, geotechnical, geophysical, topographic levelling, extensometer and  
404 inclinometer measurements, etc.) in order to analyse and manage different scale spatial  
405 data for risk analysis and mitigation (Marturià et al. 2006; Palà et al. 2006; Marturia et  
406 al. 2010). Subsidence modelling, aimed at reproducing and/or predicting displacements  
407 under certain conditions, is generally a complicated task. In Spain, DInSAR has shown  
408 to be a useful tool for calibrating and validating subsidence models. In Murcia city,  
409 affected by subsidence due groundwater withdrawal and aquitard consolidation (Mulas  
410 et al. 2003), InSAR data have been used to validate numerical geotechnical models  
411 (Herrera et al. 2009a) and to calibrate hydrological models that predict future scenarios  
412 of piezometric level change (Tomás et al. 2010a) (Figure 7). DInSAR data, jointly with  
413 in-situ measurements (piezometric level and geological-geotechnical information), are  
414 being used by the *Vega Baja and Media* of the *Segura* river local authorities for water  
415 supply management. In *Sallent*, the geometry of mining and karstic cavities in a salt  
416 formation have been modelled to match topographic levelling (López et al. 2010). In the  
417 *Sant Feliu del Llobregat* pilot site, water extraction volumes have been incorporated  
418 into geological models to match DInSAR data with water pumping points and volumes  
419 (Concha et al. 2010). In *Murcia* and *Orihuela* DInSAR data have been used for building  
420 damage mapping (Herrera et al. 2010; Bru et al. 2013; Herrera et al. 2012; Tomás et al.  
421 2012) (Figure 8). DInSAR displacement measurements have also allowed the  
422 identification of damage on buildings and other man-made structures (bridges,  
423 sidewalks, walls, etc.). This application has been substantially improved since the  
424 launch of the TerraSAR-X satellite that provides a high spatial resolution and allows

425 computing the angular distortions and the differential settlement affecting the individual  
426 buildings.

427 Recent works (Tomás et al. 2010b; Tomás et al. 2011) have analysed the influence of  
428 different triggering and conditioning factors on subsidence phenomena by integrating  
429 DInSAR data from the *Segura* River valley with multiple variables in a GIS  
430 environment. The cross analysis of the different factors and the subsidence maps reveals  
431 some interesting relationships between the different factors that influence subsidence.  
432 These findings can be used as the basis for the hydraulic management of the watershed.

433

434

435 Figure 7. Modelling of subsidence caused by groundwater withdrawal in *Murcia* city.  
436 The model has been calibrated using InSAR data for the period 1993-1995 and  
437 extrapolated for 1995-2007.

438

439

440 Figure 8. Detail of DInSAR map of *Murcia* city applied for building damage  
441 monitoring. Above: Subsidence rates measured from 1995 to 2008 (left) and from 2006  
442 to 2010 (right). Center: Cross-section depicting the surface damage observed in three  
443 adjacent buildings with different foundations along the transect X-X' indicated in the  
444 detailed DInSAR map. Below: Profile of the subsidence magnitude recorded along X-  
445 X'.

446

447 Studies conducted in the *Canary Islands* (Fernández et al. 2002; Fernández et al. 2003;  
448 Fernández et al. 2005; Fernández et al. 2009; González et al. 2010; González and

449 Fernández 2011b) have shown that DInSAR is a very powerful technique for the  
450 volcano activity monitoring in an operative and systematic way.

451 Polarimetric SAR Interferometry (PolInSAR) has been recently used by several  
452 researchers (Navarro-Sanchez et al. 2010; Navarro-Sanchez and Lopez-Sanchez 2012)  
453 in order to increase the number of PS candidates. This approach allows increasing the  
454 PS density by the identification of pixels with good phase quality after a search in the  
455 available polarimetric space.

456

457

### 458 3.6 Independent validation of the DInSAR results: measurements precision

459 Strong efforts have been done in order to assess independently the precision of the  
460 DInSAR subsidence measurements. This independent validation process is usually  
461 performed by comparing DInSAR data with in situ measurements. Consequently, in situ  
462 displacements have to be projected along the LOS in order to be able to make direct  
463 comparisons. The precision of DInSAR techniques, defined as the dispersion of the  
464 displacement estimates around the expected value, depends on a number of parameters  
465 (e.g. González and Fernández 2011b; Hooper et al. 2012) whose exposition is out of the  
466 scope of this work. However, some authors (Colesanti and Wasowski 2006; Lanari et al.  
467 2007; Raucoules et al. 2007; Prati et al. 2010; e.g. Ferretti et al. 2011; Hooper et al.  
468 2012) suggested a typical precision for average displacement rate and LOS  
469 displacements values of up to  $\pm 1$ mm/year and  $\pm 5$  mm respectively. So far, the direct  
470 comparison of DInSAR subsidence data with displacement values measured in situ is  
471 the most common way to evaluate the precision of these techniques. Some subsidence  
472 areas in Spain monitored with DInSAR have been compared with geodetic or  
473 topographical measurements (e.g. Tenerife Island; Fernández et al. 2003; 2009)

474 resulting in good sub-centimetre agreements (Figure 9). Table 3 shows the precisions of  
475 DInSAR measurements obtained by several authors.

476

477 Figure 9. (a) Comparison of subsidence measurements in Tenerife Island obtained by  
478 Small Baseline InSAR and GPS. The GPS values have been projected along the LOS  
479 for direct comparison. (b) Location of the comparison points, color-coded according to  
480 the correlation index between the time series of displacements from the two techniques.

481

482 Table 3. Estimated precision of subsidence measurements obtained with DInSAR in the  
483 analysed areas of Spain (See Figure 1 for locations). (\*) The error is computed as the  
484 average absolute difference between the in situ and InSAR measurements for the whole  
485 available data.

486

#### 487 4 Cost analysis of InSAR

488 A comparative summary of the different techniques most frequently used for measuring  
489 subsidence is presented in Table 4. The characteristics summarized for each technique  
490 include accuracy, displacement component, survey scale, conditions and characteristics  
491 of the operating environments, degree of automation and sampling frequency. A  
492 detailed description of some of these techniques employed for subsidence monitoring  
493 can be found in Galloway (1998) and Galloway and Burbey (2011).

494

495 Table 4. Comparative of method for measuring ground subsidence. G: Good; MD:  
496 Medium; P: Poor; MN: Manually; A: Automatic; SA: Semiautomatic.

497

498 A comparative study of the eight techniques used for monitoring the subsidence in 11  
499 case studies in Spain was performed for estimating their cost. Monitoring parameters  
500 not considered in Table 4, such as the temporal frequency of the measurements (time  
501 interval between consecutive measurements) and the mapped point density (number of  
502 measurements per unit area), were also included. The evaluation of the cost for the  
503 different techniques (levelling, InSAR, GPS, etc.) is heterogeneous because of the  
504 distinct operational context. For this reason we assume a similar post-processing cost  
505 for the different techniques. Therefore, the cost calculation is based on the commercial  
506 (non-scientific) SAR image price or the value of every field campaign. In the case of the  
507 geodetic station of *Lanzarote* and the automatic extensometer of *Sallent*, the value has  
508 been computed considering the annual maintenance cost of these instruments.

509 The following economic parameters have been estimated: (a) the annual cost per  
510 measurement point; (b) the difference between the annual costs of each approach and  
511 the cost using ERS-ENVISAT-based InSAR. This parameter provides an idea about  
512 how costly or inexpensive are the considered techniques in comparison with InSAR  
513 ERS-ENVISAT processing through a year; (c) the annual cost per unit area ( $\text{km}^2$ ) with  
514 respect to ERS-ENVISAT-based InSAR processing; and (d) the annual cost per  
515 measurement point relative to the price estimated for monitoring the same point by  
516 means of ERS-ENVISAT images. For all of them, the maximum, minimum and mean  
517 values have been computed.

518 The results of the analysis are shown in Figure 10. Figure 10a shows the mean  
519 measurement frequency (per year) of eight techniques considered. The acquisition  
520 frequency is crucial for identifying and analysing subsidence phenomena with non-  
521 linear or episodic kinematics. Excluding the continuous acquisition systems that are  
522 usually installed in areas affected by rapid subsidence and where a high risk for

523 population exists, the highest measurement frequencies correspond to CosmoSkyMed  
524 (up to 15 possible measurements per year) and TerraSAR-X (8.7 - 21.6 measurements  
525 per year). ERS-ENVISAT processings provide between 6 and 10 measurements per  
526 year. Usually, levelling, GPS and extensometers are used for providing 1 or 2  
527 measurements per year.

528 The point density (number of points with subsidence measurement per square  
529 kilometre) is critical for identifying the spatial subsidence patterns (Figure 10b). The  
530 highest point density is provided by the TerraSAR-X satellite (average, minimum and  
531 maximum density of 825, 701 and 916 points per square kilometre, respectively) due to  
532 its high resolution. CosmoSkyMed and the automatic total stations also provide a high  
533 point density. However, the latter has the disadvantage of measuring benchmarks  
534 located at short distances ( $< 1$  km). Levelling and ERS-ENVISAT InSAR provide a  
535 similar point density, with mean values of 93 and 51 points per square kilometre,  
536 respectively. GPS, extensometer and geodetic stations provides the lowest density of  
537 subsidence measurements, with maximum values of 4 points per square kilometre. The  
538 geodetic station has been included in the cost analysis. It is a singular laboratory located  
539 under exceptional environmental conditions which includes high-precision geodetic  
540 instrumentation (e.g., tiltmeters, strainmeters, gravimeters, GPS, etc.) with continuous  
541 acquisition data systems. The geodetic station is not only used to carry out the study of  
542 the geodynamics processes but also the instrumental research. As example, the geodetic  
543 station located in Lanzarote Island (Vieira et al. 1991; Fernández et al. 1992) includes  
544 three instrumental locations dedicated to the study of the Solid Earth deformations,  
545 Earth Tides, sea-level variations, etc.

546 A relevant parameter from the economic feasibility perspective is the annual cost per  
547 point, given by the ratio between the total annual cost of the implementation of the

548 technique in Euros, and the available number of information points. The results show  
549 that the four case studies analysed by means of TSX-InSAR provide the lowest annual  
550 cost (0.65 € per year per point) in comparison with the average cost of the eleven cases  
551 analyzed with ERS-ENVISAT-InSAR (1.20 € per year and point), and the remaining  
552 techniques (Figure 10c). Levelling, extensometers and GPS have the highest prices per  
553 measurement point and year, ranging from 220 to 1007 Euros. Figure 10f shows the  
554 annual cost per measurement point compared with InSAR. Although TSX-InSAR  
555 provides the lowest mean cost per point (Figure 10c), the relative cost per point is lower  
556 for the three case studies where both sensors (ERS-ENVISAT and TSX) were used.

557 The annual costs of the different techniques has been also computed and compared with  
558 that of the ERS-ENVISAT-InSAR (Figure 10d). Obviously, this cost strongly depends  
559 on the number of measurements obtained each year, especially for instrumental  
560 techniques (extensometers and levelling) and for GPS. For this reason, the  
561 extensometers installed over a salt mine in *Sallent, Barcelona*, which provide a  
562 continuous record (8,760 measurements per year) have not been considered in the  
563 analyses. The results show that most of the techniques considered are from 4 to 10 times  
564 more expensive than ERS-ENVISAT-InSAR. However, TSX-InSAR and GPS provides  
565 the highest mean annual costs (22 and 26 times higher, respectively).

566 Figure 10e shows the annual cost per square kilometre of each technique compared with  
567 that of ERS-ENVISAT-InSAR. These estimates depend to a large extent on the area  
568 extent surveyed. The InSAR techniques yield the lowest annual cost per square  
569 kilometre, in addition to their high point density, as mentioned above. The geodetic  
570 stations provide a low cost (6 times higher than ERS-ENVISAT-InSAR) because the  
571 whole Lanzarote Island (845 km<sup>2</sup>) is monitored with only 3 measurement points.  
572 Consequently, in this case, although the annual cost unit per square kilometre is low, the

573 spatial density of data is very poor. Due to the coverage of SAR images (100×100,  
574 30×50 and 20×20 km for ERS-ENVISAT, TSX and CosmoSkyMed, respectively),  
575 DInSAR techniques are considered of low-cost for large study areas.

576

577 Figure 10. Comparative cost analysis of the eight techniques used for measuring the  
578 subsidence in Spain. See explanation in the text. (\*) The continuous record of the  
579 extensometer installed in *Sallent* has not been considered for mean estimation. (\*\*) The  
580 measuring network extends partially within the area with DInSAR detected movements  
581 and it has set focusing in areas with detected intensive subsidence.

582

583

#### 584 5 Concluding remarks

585 Since the first application of DInSAR to identify soil swelling (Gabriel et al. 1989), this  
586 useful technique has become a widespread tool for subsidence monitoring, providing a  
587 high amount of ground displacement data for wide areas and at low cost compared with  
588 ground-based techniques. Nineteen subsidence areas (mining, groundwater withdrawal,  
589 evaporite dissolution, volcanism and load-induced compaction) in Spain have been  
590 recognized and/or studied using DInSAR techniques during the last twenty years. In  
591 some cases, DInSAR has allowed the identification of previously unknown subsidence  
592 areas providing information on distribution and rate of the settlement process. In other  
593 cases, DInSAR has been used as a tool for the analysis, modelling and management of  
594 potentially hazardous subsidence processes in combination with other complementary  
595 information. The principal limitations of DInSAR techniques are the loss of coherence  
596 between two acquisitions caused by temporal decorrelation (especially in agricultural  
597 and vegetated areas), the atmospheric artefacts that affect the displacement estimation,



598 the availability of images that depends on the satellites repeat-orbit cycle, and the low  
599 capability to measure horizontal displacements. However, the main advantages of  
600 DInSAR are the high performance measuring vertical displacements, the low cost in  
601 comparison with other techniques especially when studying large areas, the short  
602 revisiting period compared to field techniques, the large spatial coverage, the ability to  
603 operate even at night or under adverse weather conditions, and the possibility of  
604 analysing areas retrospectively using historical data since 1992 using the ESA's SAR  
605 archives. The cost analysis performed has allowed us to identify the strongest points of  
606 the InSAR techniques compared with other conventional techniques: (1) higher data  
607 acquisition frequency and spatial coverage; and (2) lower annual cost per measurement  
608 point and per square kilometre. The obtained results show that in many cases the clear  
609 advantages of DInSAR compensate and even get over the limitations of this technique.

610 In Spain more than ten different DInSAR techniques have been used for the study of  
611 subsidence phenomena. Although advanced techniques are widely used due to their  
612 capability to minimize atmospheric artefacts, in some cases, conventional DInSAR  
613 techniques are required due to the high velocity of the subsidence. As a consequence,  
614 DInSAR has become an indispensable tool to satisfactorily address many subsidence  
615 studies. In the future, the development of new algorithms, the launch of new satellites,  
616 the integration InSAR data with ground-based measurements and the joint performance  
617 of ground and airborne platforms will allow improving substantially the resolution and  
618 precision of DInSAR techniques and the monitoring and managing of ground  
619 subsidence hazards.

620

621 Acknowledgements

622 Authors thank O. Monserrat and M. Crosetto (Institut de Geomàtica) for their useful  
623 comments and the review of first version of the manuscript. The ERS and ENVISAT  
624 images mentioned in this work were provided by the European Space Agency (ESA) in  
625 the framework of the EO Cat.1-2494 and Cat.1-3462 projects and the Terrafirma GMES  
626 Project. The TerraSAR-X images were provided by DLR in the framework of the  
627 scientific project GEO0389. The different research areas included in this paper has been  
628 supported by the projects: CGL2005-05500-C02, CGL2008-06426-C01-01/BTE,  
629 AYA2010-17448, IPT-2011-1234-310000, TEC-2008-06764, ACOMP/2010/082,  
630 AGL2009-08931/AGR, 2012GA-LC-036, 2003-03-4.3-I-014, CGL2006-05415, BEST-  
631 2011/225, CGL2010-16775, TEC2011-28201, 2012GA-LC-021 and the Banting  
632 Postdoctoral Fellowship to PJG. This research is a contribution of the Moncloa Campus  
633 of International Excellence (UCM-UPM, CSIC).

634

## 635 References

- 636 Arnaud A, Adam N, Hanssen R, Inglada J, Duro J, Closa J, Eineder M ASAR ERS  
637 interferometric phase continuity. In: Geoscience and Remote Sensing  
638 Symposium, 2003. IGARSS '03. Proceedings. 2003 IEEE International, 21-25  
639 July 2003 2003. pp 1133-1135 vol.1132. doi:10.1109/igarss.2003.1294035
- 640 Autin WJ (2002) Landscape evolution of the Five Islands of south Louisiana: scientific  
641 policy and salt dome utilization and management. *Geomorphology* 47 (2-  
642 4):227-244. doi:10.1016/s0169-555x(02)00086-7
- 643 Bamler R, Hartl P (1998) Synthetic aperture radar interferometry. *Inverse Problems* 14  
644 (4):R1
- 645 Berardino P, Fornaro G, Lanari R, Sansosti E (2002) A new algorithm for surface  
646 deformation monitoring based on small baseline differential SAR  
647 interferograms. *Geoscience and Remote Sensing, IEEE Transactions on* 40  
648 (11):2375-2383. doi:10.1109/tgrs.2002.803792
- 649 Blanco P, Arbiol R, Palà V (2008) ALOS-PALSAR performances on a multiple sensor  
650 DInSAR scenario for deformation monitoring applications. Paper presented at  
651 the ALOS 2008 Symposium, Rhodes, Greece, 3-7 November
- 652 Bru G, Herrera G, Tomás R, Duro J, De la Vega R, Mulas J (2013) Control of  
653 deformation of buildings affected by subsidence using persistent scatterer  
654 interferometry. *Structure and Infrastructure Engineering* 9:188-200.  
655 doi:10.1080/15732479.2010.519710
- 656 Castañeda C, Gutiérrez F, Galve JP, Pourthié N, Souyris JC, Manunta M (2009a)  
657 Comparación de dos técnicas de interferometría radar mediante deformaciones

658 generadas por disolución de evaporitas, minería y deslizamientos (Valle del  
659 Ebro, España). In: Montesinos S, Fernández L (eds) Teledetección: agua y  
660 desarrollo sostenible. Zaragoza, Spain, pp 261-264

661 Castañeda C, Gutiérrez F, Manunta M, Galve JP (2009b) DInSAR measurements of  
662 ground deformation by sinkholes, mining subsidence, and landslides, Ebro  
663 River, Spain. *Earth Surface Processes and Landforms* 34 (11):1562-1574.  
664 doi:10.1002/esp.1848

665 Castañeda C, Pourthie' N, Souyris J-C (2011) Dedicated SAR interferometric analysis  
666 to detect subtle deformation in evaporite areas around Zaragoza, NE Spain.  
667 *International Journal of Remote Sensing* 32 (7):1861-1884.  
668 doi:10.1080/01431161003631584

669 Colesanti C, Wasowski J (2006) Investigating landslides with space-borne Synthetic  
670 Aperture Radar (SAR) interferometry. *Engineering Geology* 88 (3-4):173-199.  
671 doi:10.1016/j.enggeo.2006.09.013

672 Concha A, Ripoll J, Piña J, Gabàs A, Piña E (2010) Two-dimensional coupled  
673 numerical modelling of subsidence due to water extraction at the Lower  
674 Llobregat River, Spain. Paper presented at the Land Subsidence, Associated  
675 Hazards and the Role of Natural Resources Development. Proceedings of  
676 EISOLS 2010, Querétaro, Mexico,

677 Corapcioglu MY (1989) Land subsidence a state of the art review. In: Bear M,  
678 Corapcioglu MY (eds) *Fundamentals of Transport Phenomena in Porous Media*.  
679 Nato, A.S.I. Series. Martinus Nijhoff Publishers, Dordrecht, Netherlands, pp  
680 369-444

681 Crosetto M, Crippa B, Biescas E (2005a) Early detection and in-depth analysis of  
682 deformation phenomena by radar interferometry. *Engineering Geology* 79 (1-  
683 2):81-91. doi:10.1016/j.enggeo.2004.10.016

684 Crosetto M, Crippa B, Biescas E, Monserrat O, Agudo M, Fernández P (2005b) Land  
685 deformation monitoring using SAR interferometry: State-of-the-art.  
686 *Photogrammetrie, Fernerkundung, Geoinformation* 6:497-510

687 Crosetto M, Monserrat O, Iglesias R, Crippa B (2010) Persistent Scatterer  
688 Interferometry: potential, limits and initial C- and X-band comparison.  
689 *Photogrammetric Engineering and Remote Sensing* 76 (9):9

690 De Bruyn IA, Bell FG (2001) The occurrence of sinkholes and subsidence depressions  
691 in the far west Rand and Gauteng Province, South Africa, and their engineering  
692 implications. *Environmental & Engineering Geoscience* 7 (3):281-295.  
693 doi:10.2113/gseegeosci.7.3.281

694 Fernández J, Romero R, Carrasco D, Luzón F, Araña V (2002) InSAR volcano and  
695 seismic monitoring in Spain. Results for the period 1992-2000 and possible  
696 interpretations. *Optics and Lasers in Engineering* 37 (2-3):285-297.  
697 doi:10.1016/s0143-8166(01)00085-9

698 Fernández J, Romero R, Carrasco D, Tiampo KF, Rodríguez-Velasco G, Aparicio A,  
699 Araña V, González-Matesanz FJ (2005) Detection of displacements on Tenerife  
700 Island, Canaries, using radar interferometry. *Geophysical Journal International*  
701 160 (1):33-45. doi:10.1111/j.1365-246X.2005.02487.x

702 Fernández J, Tizzani P, Manzo M, Borgia A, González PJ, Martí J, Pepe A, Camacho  
703 AG, Casu F, Berardino P, Prieto JF, Lanari R (2009) Gravity-driven deformation  
704 of Tenerife measured by InSAR time series analysis. *Geophys Res Lett* 36  
705 (4):L04306. doi:10.1029/2008gl036920

- 706 Fernández J, Vieira R, Díez JL, Toro C (1992) Investigations on crustal thickness, heat  
707 flow and gravity tide relationship in Lanzarote Island. *Physics of the Earth and*  
708 *Planetary Interiors* 74 (3-4):10. doi:10.1016/0031-9201(92)90010-S
- 709 Fernández J, Yu TT, Rodríguez-Velasco G, González-Matesanz J, Romero R,  
710 Rodríguez G, Quirós R, Dalda A, Aparicio A, Blanco MJ (2003) New geodetic  
711 monitoring system in the volcanic island of Tenerife, Canaries, Spain.  
712 Combination of InSAR and GPS techniques. *Journal of Volcanology and*  
713 *Geothermal Research* 124 (3–4):241-253. doi:10.1016/s0377-0273(03)00073-8
- 714 Fernandez P, Irigaray C, Jimenez J, El Hamdouni R, Crosetto M, Monserrat O, Chacon  
715 J (2009) First delimitation of areas affected by ground deformations in the  
716 Guadalfeo River Valley and Granada metropolitan area (Spain) using the  
717 DInSAR technique. *Engineering Geology* 105 (1–2):84-101.  
718 doi:10.1016/j.enggeo.2008.12.005
- 719 Ferretti A, Prati C, Rocca F (2001) Permanent scatterers in SAR interferometry.  
720 *Geoscience and Remote Sensing, IEEE Transactions on* 39 (1):8-20.  
721 doi:10.1109/36.898661
- 722 Ferretti A, Tamburini A, Novali F, Fumagalli A, Falorni G, Rucci A (2011) Impact of  
723 high resolution radar imagery on reservoir monitoring. *Energy Procedia* 4  
724 (0):3465-3471. doi:10.1016/j.egypro.2011.02.272
- 725 Gabriel AK, Goldstein RM, Zebker HA (1989) Mapping Small Elevation Changes Over  
726 Large Areas: Differential Radar Interferometry. *J Geophys Res* 94 (B7):9183-  
727 9191. doi:10.1029/JB094iB07p09183
- 728 Galve JP, Gutiérrez F, Guerrero J, Alonso J, Diego I (2012) Optimizing the application  
729 of geosynthetics to roads in sinkhole-prone areas on the basis of hazard models  
730 and cost-benefit analyses. *Geotextiles and Geomembranes* 34 (0):80-92.  
731 doi:10.1016/j.geotexmem.2012.02.010
- 732 Galloway D, Burbey T (2011) Review: Regional land subsidence accompanying  
733 groundwater extraction. *Hydrogeology Journal* 19 (8):1459-1486.  
734 doi:10.1007/s10040-011-0775-5
- 735 Galloway DL, Hudnut KW, Ingebritsen SE, Phillips SP, Peltzer G, Rogez F, Rosen PA  
736 (1998) Detection of aquifer system compaction and land subsidence using  
737 interferometric synthetic aperture radar, Antelope Valley, Mojave Desert,  
738 California. *Water Resour Res* 34 (10):2573-2585. doi:10.1029/98wr01285
- 739 Galloway DL, Jones DR, Ingebritsen SE (eds) (1999) *Land Subsidence in the United*  
740 *States U.S. Geological Survey Circular vol 1182.* U.S. Geological Survey,  
741 Reston, Virginia
- 742 Gonzalez de Vallejo L, Ferrer M (2011) *Geological Engineering 1edn.*,
- 743 González PJ, Fernández J (2011a) Drought-driven transient aquifer compaction imaged  
744 using multitemporal satellite radar interferometry. *Geology*.  
745 doi:10.1130/g31900.1
- 746 González PJ, Fernández J (2011b) Error estimation in multitemporal InSAR  
747 deformation time series, with application to Lanzarote, Canary Islands. *J*  
748 *Geophys Res* 116 (B10):B10404. doi:10.1029/2011jb008412
- 749 González PJ, Tiampo KF, Camacho AG, Fernández J (2010) Shallow flank deformation  
750 at Cumbre Vieja volcano (Canary Islands): Implications on the stability of steep-  
751 sided volcano flanks at oceanic islands. *Earth and Planetary Science Letters* 297  
752 (3–4):545-557. doi:10.1016/j.epsl.2010.07.006
- 753 Guerrero J, Gutiérrez F, Bonachea J, Lucha P (2008) A sinkhole susceptibility zonation  
754 based on paleokarst analysis along a stretch of the Madrid–Barcelona high-speed

755 railway built over gypsum- and salt-bearing evaporites (NE Spain). *Engineering*  
756 *Geology* 102 (1–2):62-73. doi:10.1016/j.enggeo.2008.07.010

757 Gutiérrez F, Galve J, Lucha P, Bonachea J, Jordá L, Jordá R (2009) Investigation of a  
758 large collapse sinkhole affecting a multi-storey building by means of geophysics  
759 and the trenching technique (Zaragoza city, NE Spain). *Environmental Geology*  
760 58 (5):1107-1122. doi:10.1007/s00254-008-1590-8

761 Hanssen RF (2001) *Radar Interferometry. Data Interpretation and Error Analysis*, vol 2.  
762 *Remote Sensing and Digital Image Processing*. Springer,

763 Henderson FM, Lewis AJ (eds) (1998) *Principles and Application of Imaging Radar.*  
764 *Manual of Remote Sensing*, vol 2. John Wiley and Sons, New York, US

765 Herrera G, Álvarez Fernández MI, Tomás R, González-Nicieza C, López-Sánchez JM,  
766 Álvarez Vigil AE (2012) Forensic analysis of buildings affected by mining  
767 subsidence based on Differential Interferometry (Part III). *Engineering Failure*  
768 *Analysis* 24 (0):67-76. doi:10.1016/j.engfailanal.2012.03.003

769 Herrera G, Fernández JA, Tomás R, Cooksley G, Mulas J (2009a) Advanced  
770 interpretation of subsidence in Murcia (SE Spain) using A-DInSAR data –  
771 modelling and validation. *Nat Hazards Earth Syst Sci* 9 (3):647-661.  
772 doi:10.5194/nhess-9-647-2009

773 Herrera G, Tomás R, Lopez-Sanchez JM, Delgado J, Mallorqui JJ, Duque S, Mulas J  
774 (2007) Advanced DInSAR analysis on mining areas: La Union case study  
775 (Murcia, SE Spain). *Engineering Geology* 90 (3-4):148-159

776 Herrera G, Tomás R, Lopez-Sanchez JM, Delgado J, Vicente F, Mulas J, Cooksley G,  
777 Sanchez M, Duro J, Arnaud A, Blanco P, Duque S, Mallorqui JJ, De la Vega-  
778 Panizo R, Monserrat O (2009b) Validation and comparison of Advanced  
779 Differential Interferometry Techniques: Murcia metropolitan area case study.  
780 *ISPRS Journal of Photogrammetry and Remote Sensing* 64 (5):501-512

781 Herrera G, Tomás R, Monells D, Centolanza G, Mallorquí JJ, Vicente F, Navarro VD,  
782 Lopez-Sanchez JM, Sanabria M, Cano M, Mulas J (2010) Analysis of  
783 subsidence using TerraSAR-X data: Murcia case study. *Engineering Geology*  
784 116 (3-4):284-295

785 Hooper A, Bekaert D, Spaans K, Arıkan M (2012) Recent advances in SAR  
786 interferometry time series analysis for measuring crustal deformation.  
787 *Tectonophysics* 514–517 (0):1-13. doi:10.1016/j.tecto.2011.10.013

788 Jackson JA (1997) *Glossary of Geology* 4th edn. American Geological Institute,  
789 Alexandria, Virginia, US

790 Kampes BM (2006) *Radar Interferometry. Persistent Scatterer Technique*, vol 12.  
791 *Remote Sensing and Digital Image Processing*. Springer,

792 Kappel WM, Yager RM, Todd MS (1999) The Retsof Salt Mine Collapse. In: Galloway  
793 DL, Jones DR, Ingebritsen SE (eds) *Land Subsidence in the United States*, vol  
794 1182. vol US Geological Survey Circular. US Geological Survey, Reston,  
795 Virginia, pp 111-120

796 Lanari R, Casu F, Manzo M, Zeni G, Berardino P, Manunta M, Pepe A (2007) An  
797 Overview of the Small BAseline Subset Algorithm: A DInSAR Technique for  
798 Surface Deformation Analysis. In: Wolf D, Fernández J (eds) *Deformation and*  
799 *Gravity Change: Indicators of Isostasy, Tectonics, Volcanism, and Climate*  
800 *Change. Pageoph Topical Volumes*. Birkhäuser Basel, pp 637-661.  
801 doi:10.1007/978-3-7643-8417-3\_2

802 López F, Buxó P, Palau J, Marturià J, Concha A, Martínez P (2010) Evaluation of the  
803 subsidence and risk of collapse in the estació neighbourhood of the Sallent City  
804 (Spain). Paper presented at the Land Subsidence, Associated Hazards and the

805 Role of Natural Resources Development. Proceedings of EISOLS 2010,  
806 Querétaro, Mexico,

807 Lundgren P, Usai S, Sansosti E, Lanari R, Tesauro M, Fornaro G, Berardino P (2001)  
808 Modeling surface deformation observed with synthetic aperture radar  
809 interferometry at Campi Flegrei caldera. *J Geophys Res* 106 (B9):19355-19366.  
810 doi:10.1029/2001jb000194

811 Mancini F, Stecchi F, Zanni M, Gabbianelli G (2009) Monitoring ground subsidence  
812 induced by salt mining in the city of Tuzla (Bosnia and Herzegovina).  
813 *Environmental Geology* 58 (2):381-389. doi:10.1007/s00254-008-1597-1

814 Marturià J, de Diego J, Martínez P, Roca A (2006) Implementation of a subsidence risk  
815 management system. Paper presented at the 5th European Congress on Regional  
816 Geoscience Cartography and Informations Systems, Barcelona,

817 Marturia J, Ripoll J, Concha A, Barberà M (2010) Monitoring techniques for analysing  
818 subsidence: a basis for implementing an Early Warning System. Paper presented  
819 at the Land Subsidence, Associated Hazards and the Role of Natural Resources  
820 Development. Proceedings of EISOLS 2010, Querétaro, Mexico,

821 Massonnet D, Feigl KL (1998) Radar interferometry and its application to changes in  
822 the Earth's surface. *Rev Geophys* 36 (4):441-500. doi:10.1029/97rg03139

823 Massonnet D, Rossi M, Carmona C, Adragna F, Peltzer G, Feigl K, Rabaute T (1993)  
824 The displacement field of the Landers earthquake mapped by radar  
825 interferometry. *Nature* 364 (6433):138-142

826 Monserrat O (2012) Deformation measurement and monitoring with Ground-Based  
827 SAR. Universitat Politècnica de Catalunya, Barcelona

828 Mora O, Arbiol R, Palà V (2007) The experience of the cartographic Institute of  
829 Catalonia (ICC) on continuous DInSAR monitoring of large areas. Paper  
830 presented at the Envisat Symposium 2007, Montreux, Switzerland,

831 Mora O, Mallorqui JJ, Broquetas A (2003) Linear and nonlinear terrain deformation  
832 maps from a reduced set of interferometric SAR images. *Geoscience and  
833 Remote Sensing, IEEE Transactions on* 41 (10):2243-2253

834 Mulas J, Aragón R, Martínez M, Lambán J, García-Aróstegui JL, Fernández-Grillo AI,  
835 Hornero J, Rodríguez J, Rodríguez JM (2003) Geotechnical and hydrogeological  
836 analysis of land subsidence in Murcia (Spain). *Materials and Geoenvironment*  
837 50:249-252

838 Navarro-Sanchez VD, Lopez-Sanchez JM (2012) Improvement of Persistent-Scatterer  
839 Interferometry Performance by Means of a Polarimetric Optimization.  
840 *Geoscience and Remote Sensing Letters, IEEE* 9 (4):609-613.  
841 doi:10.1109/lgrs.2011.2176715

842 Navarro-Sanchez VD, Lopez-Sanchez JM, Vicente-Guijalba F (2010) A Contribution of  
843 Polarimetry to Satellite Differential SAR Interferometry: Increasing the Number  
844 of Pixel Candidates. *Geoscience and Remote Sensing Letters, IEEE* 7 (2):276-  
845 280. doi:10.1109/lgrs.2009.2033013

846 Oller P, Gonzalez M, Pinyol J, Marturià J, Martínez P (2011) Geohazards Mapping in  
847 Catalonia. *Journal Torrent, Avalanche, Landslide Rock Fall Engineering* 74:8

848 Palà V, Mora O, Arbiol R, Marturià J (2006) Products derived from an advanced  
849 DInSAR-GIS application for risk management. In: ISPRS (ed) *Geospatial  
850 databases for sustainable development*. Goa, India, p 5

851 Peltzer G, Rosen P (1995) Surface Displacement of the 17 May 1993 Eureka Valley,  
852 California, Earthquake Observed by SAR Interferometry. *Science* 268  
853 (5215):1333-1336. doi:10.1126/science.268.5215.1333

- 854 Pipia L, Aguasca A, Fabregas X, Mallorqui JJ, Lopez-Martinez C, Marturia J Mining  
855 Induced Subsidence Monitoring in Urban Areas with a Ground-Based SAR. In:  
856 Urban Remote Sensing Joint Event, 2007, 11-13 April 2007 2007. pp 1-5.  
857 doi:10.1109/urs.2007.371881
- 858 Pipia L, Fabregas X, Aguasca A, Duque S, Mallorqui JJ, Lopez-Martinez C  
859 Polarimetric Deformation Maps Retrieval of Urban Areas using Ground-Based  
860 SAR Acquisitions. In: Geoscience and Remote Sensing Symposium, 2008.  
861 IGARSS 2008. IEEE International, 7-11 July 2008 2008. pp IV - 327-IV - 330.  
862 doi:10.1109/igarss.2008.4779724
- 863 Prati C, Ferretti A, Perissin D (2010) Recent advances on surface ground deformation  
864 measurement by means of repeated space-borne SAR observations. *Journal of*  
865 *Geodynamics* 49 (3–4):161-170. doi:10.1016/j.jog.2009.10.011
- 866 Prokopovich NP (1979) Genetic classification on land subsidence. Paper presented at  
867 the International Conference on Evaluation and Prediction of Subsidence,  
868 Pensacola Beach, Florida,
- 869 Pulido-Bosch A, Delgado J, Sola F, Vallejos Á, Vicente F, López-Sánchez JM,  
870 Mallorquí JJ (2011) Identification of potential subsidence related to pumping in  
871 the Almería basin (SE Spain). *Hydrological Processes* 26 (5):731-740.  
872 doi:10.1002/hyp.8181
- 873 Raucoules D, Colesanti C, Carnec C (2007) Use of SAR interferometry for detecting  
874 and assessing ground subsidence. *Comptes Rendus Geoscience* 339 (5):289-302.  
875 doi:10.1016/j.crte.2007.02.002
- 876 Rodríguez-Estrella T, Manteca JL, García C (2000) Subsistencia minera, en relación con  
877 sismotectónica, en La Unión (Murcia). *Geotemas* 1:150-153
- 878 Sansosti E, Casu F, Manzo M, Lanari R (2010) Space-borne radar interferometry  
879 techniques for the generation of deformation time series: An advanced tool for  
880 Earth's surface displacement analysis. *Geophys Res Lett* 37 (20):L20305.  
881 doi:10.1029/2010gl044379
- 882 Schmidt DA, Bürgmann R (2003) Time-dependent land uplift and subsidence in the  
883 Santa Clara valley, California, from a large interferometric synthetic aperture  
884 radar data set. *J Geophys Res* 108 (B9):2416. doi:10.1029/2002jb002267
- 885 Simons M, Rosen PA (2007) 3.12 - Interferometric Synthetic Aperture Radar Geodesy.  
886 In: Editor-in-Chief: Gerald S (ed) *Treatise on Geophysics*. Elsevier,  
887 Amsterdam, pp 391-446
- 888 Sousa JJ, Ruiz AM, Hanssen RF, Bastos L, Gil AJ, Galindo-Zaldívar J, Sanz de  
889 Galdeano C (2010) PS-InSAR processing methodologies in the detection of field  
890 surface deformation—Study of the Granada basin (Central Betic Cordilleras,  
891 southern Spain). *Journal of Geodynamics* 49 (3–4):181-189.  
892 doi:<http://dx.doi.org/10.1016/j.jog.2009.12.002>
- 893 Tomás R, García-Barba J, Cano M, Sanabria MP, Ivorra S, Duro J, Herrera G (2012)  
894 Subsidence damage assessment of a gothic church using Differential  
895 Interferometry and field data. *Structural Health Monitoring* Accepted, in press
- 896 Tomás R, Herrera G, Cooksley G, Mulas J (2011) Persistent Scatterer Interferometry  
897 subsidence data exploitation using spatial tools: The Vega Media of the Segura  
898 River Basin case study. *Journal of Hydrology* 400 (3-4):411-428
- 899 Tomás R, Herrera G, Delgado J, Lopez-Sanchez JM, Mallorquí JJ, Mulas J (2010a) A  
900 ground subsidence study based on DInSAR data: Calibration of soil parameters  
901 and subsidence prediction in Murcia City (Spain). *Engineering Geology* 111 (1-  
902 4):19-30

- 903 Tomás R, Herrera G, Lopez-Sanchez JM, Vicente F, Cuenca A, Mallorquí JJ (2010b)  
904 Study of the land subsidence in Orihuela City (SE Spain) using PSI data:  
905 Distribution, evolution and correlation with conditioning and triggering factors.  
906 Engineering Geology 115 (1-2):105-121
- 907 Tomás R, Lopez-Sanchez JM, Delgado J, Mallorquí JJ, Herrera G (2008) DInSAR  
908 monitoring of aquifer compaction due to water withdrawal: Vega Baja and  
909 Media of the Segura river (SE, Spain) case study. In: Sánchez JM (ed) Drought:  
910 causes, effects and predictions. NOVA publishers, New York, pp 253-276
- 911 Tomás R, Lopez-Sanchez JM, Delgado J, Vicente F, Cuenca A, Mallorquí JJ, Blanco P,  
912 Duque S DInSAR monitoring of land subsidence in Orihuela City, Spain:  
913 Comparison with geotechnical data. In: Geoscience and Remote Sensing  
914 Symposium, 2007. IGARSS 2007. IEEE International, 23-28 July 2007 2007. pp  
915 3027-3030
- 916 Ulaby FT, Moore RK, Fung AK (1982) Microwave Remote Sensing: Active and  
917 Passive. Advanced Book Program. Addison-Wesley, Massachusetts, US
- 918 Vieira R, Van Ruymbeke M, Fernández J, Arnosó J, Toro C (1991) The Lanzarote  
919 underground laboratory. In: van Ruymbeke M, d'Oreye N (eds) Geodynamical  
920 Instrumentation applied to Volcanic Areas, vol 4. Cahiers du Centre Européen  
921 de Géodynamique et de Séismologie, Walferdange, Grand-Duchy of  
922 Luxembourg, pp 71-86
- 923 Waltham T (1989) Ground subsidence. Chapman & Hall, New York, US
- 924 Werner C, Wegmuller U, Strozzi T, Wiesmann A Interferometric point target analysis  
925 for deformation mapping. In: Geoscience and Remote Sensing Symposium,  
926 2003. IGARSS '03. Proceedings. 2003 IEEE International, 21-25 July 2003  
927 2003. pp 4362-4364 vol.4367. doi:10.1109/igarss.2003.1295516
- 928 Wu Y (2003) Mechanism analysis of hazards caused by the interaction between  
929 groundwater and geo-environment. Environmental Geology 44 (7):811-819.  
930 doi:10.1007/s00254-003-0819-9  
931  
932  
933



1 **Table 1.** Radar systems employed in the reported subsidence studies in Spain. ESA:  
2 European Space Agency; DLR: German Aerospace Center; JAXA: Japan Aerospace  
3 Exploration Agency; UPC: Universidad Polit cnica de Catalu a; IG: Institut de  
4 Geom tica; ASI: Italian Space Agency.

Satellite- and ground-based SAR systems	Agency / Institution	Start- End	Band	Wavelength (cm)	Revisiting period (days)	Resolution (azimuth x range)
ERS 1-SAR	ESA	1991-2000	C	5.6	35	4 m x 20 m
ERS 2-SAR	ESA	1995-2010	C	5.6	35	4 m x 20 m
ENVISAT-ASAR	ESA	2002-2011	C	5.6	35	4 m x 20 m
TerraSAR-X	DLR	2007-2012	X	3.1	11	2 m x 3 m
ALOS-PALSAR	JAXA	2005-	L	23.6	46	10 m x 10 m
GBSAR	UPC	2007	X	3.1	User-defined	0.5 m x 0.5 m
	IG	2008-	Ku	1.8	User-defined	0.5 m x 0.0044 rad
Cosmo-Skymed-1	ASI	2007-	X	3.1	< 24 hours	< 1 m x 1 m

5

6

7 **Table 2.** DInSAR technique and pixel selection criteria implemented in the software  
8 packages applied to study subsidence in Spain. Software developer is also indicated.

<b>Technique</b>	<b>Pixel selection criteria</b>	<b>Software name</b>	<b>Developer</b>
Conventional DInSAR	Coherence	DIAPASON (Differential Interferometric Automated Process Applied to Survey Of Nature)	Centre National de la Recherche Scientifique, France
		SARscape	SARMAP, Switzerland
		DORIS (Delft Object-Oriented Radar Interferometry Software)	Technical University of Technology, The Netherlands
		EPSIE	Indra, Spain
Advanced DInSAR	Amplitude	SPN (Stable Point Network )	Altamira Information, Spain
		Delft PSI software	Technical University of Technology, The Netherlands
	Amplitude and coherence	IGPSI (Persistent Scatters Interferometry chain of the Institute of Geomatics)	Instituto de Geomática, Spain
	Coherence	CPT (Coherent Pixel Technique)	Universidad Politécnica de Cataluña, Spain
		DISSIC	Instituto Cartográfico de Cataluña, Spain
		SBAS (Small Baseline)	Institute for Electromagnetic Sensing of the Environment (IREA-CNR.), Italy
		Coherent Target Monitoring	Atlantis Scientific Inc., US.
		Interferometric Stacking	Instituto de Astronomía y Geodesia, Spain
		Multi-Temporal InSAR Analysis Package (MTIANPAC)	Instituto de Astronomía y Geodesia, Spain
	Phase stability	Stanford Method for Persistent Scatterers (StaMPS)	Stanford University, US

9

10

11

12 **Table 3.** Estimated precision of subsidence measurements obtained with DInSAR in the  
 13 analysed areas of Spain (See Figure 1 for locations). (\*) The error is computed as the  
 14 average absolute difference between the in situ and InSAR measurements for the whole  
 15 available data.

<b>Study site</b>	<b>Field complementary measurements</b>	<b>Period studied</b>	<b>Error (*)</b>
Barcelona (Sant Feliu de Llobregat pilot site)	Levelling	2008-pres.	$\pm 2$ mm
Cambrils	Levelling	2008-pres.	$\pm 2$ mm
Cardona	GPS	1997-pres.	50 mm
Cardona	Levelling	2006-pres.	$\pm 1.2$ mm
Girona	Levelling	2008-2010	$\pm 2$ mm
La Palma	GPS	1994-2008	$\leq 10$ mm
La Unión	Levelling	2003-2004	$5.0 \pm 3.0$ mm
	Extensometers	2003-2010	-
Sabadell-Sant Quirze del Vallès	Levelling	2008-2010	$\pm 2$ mm
Sallent	Levelling	1997-2004	$< 2$ mm / year
	Extensometers	2004-2010	$\pm 0.1$ mm
	Inclinometers	2008-2010	0.01 mm / 500 mm
	GB-SAR	2006-2007	
Santa Perpetua de Mogoda	Levelling	2008-pres	$\pm 2$ mm
Súria	GPS	2006-2008	12 mm
Tenerife	GPS	1994-2007	$\leq 10$ mm
Vega Media of the Segura River Basin	Extensometers	2001-2005	$5.0 \pm 2.8$ mm
		2001-2007	$3.9 \pm 3.8$ mm
		2001-2003	$< 2.4$ mm
		2000-2007	$4.5 \pm 4.1$ mm

16 3 **Table 4.** Comparative of method for measuring ground subsidence. G: Good; MD: Medium; P: Poor; MN: Manually; A: Automatic; SA:  
17 Semiautomatic.

Method	Precision	Displacement component	Survey scale	Conditions and operating environment						Degree of automation		Usual sample frequency
				<i>Rural (woody)</i>	<i>Rural (scrub)</i>	<i>Urban</i>	<i>Hilly</i>	<i>Adverse weather conditions</i>	<i>Nocturnal</i>	<i>Data acquisition</i>	<i>Post-processing</i>	
Trigonometric levelling	cm	Vertical	Line network	MD-P	MD-P	G-MD	G	P	P	MN	SA	Monthly-annual
Geometric levelling	mm	Vertical	Line network	MD-P	MD-P	G-MD	P	P	P	MN	SA	Monthly-annual
Settlement cell	mm	Vertical	Point	G	G	G	G	MD-G	MD-G	MN-A	MN-SA	Monthly-continuous
Borehole extensometer	mm	Vertical	Point	G	G	G	G	MD-G	MD-G	MN-A	MN-SA	Monthly-continuous
Differential GPS	mm	Vertical and horizontal	Point	MD-P	G-MD	MD-P	G	G-P	G	MN-A	MN-A	Monthly-annual (or continuous)
Conventional DInSAR	mm	Range	Map pixel	P	MD-P	G	G-MD	G	G	A	SA-A	Monthly-weekly (variable)
Advanced DInSAR	mm	Range	Map pixel	MD-P	MD-P	G	G-MD	G	G	A	SA-A	Monthly-weekly (variable)
GBSAR	mm	Range	Map pixel	MD-P	MD-P	G	G	G	G	A	SA-A	Hourly-daily
LIDAR/ALS/ALTM	dm	Range	Map pixel	MD	MD	G	G	MD-P	G-MD	A	SA-A	Monthly-annual

18

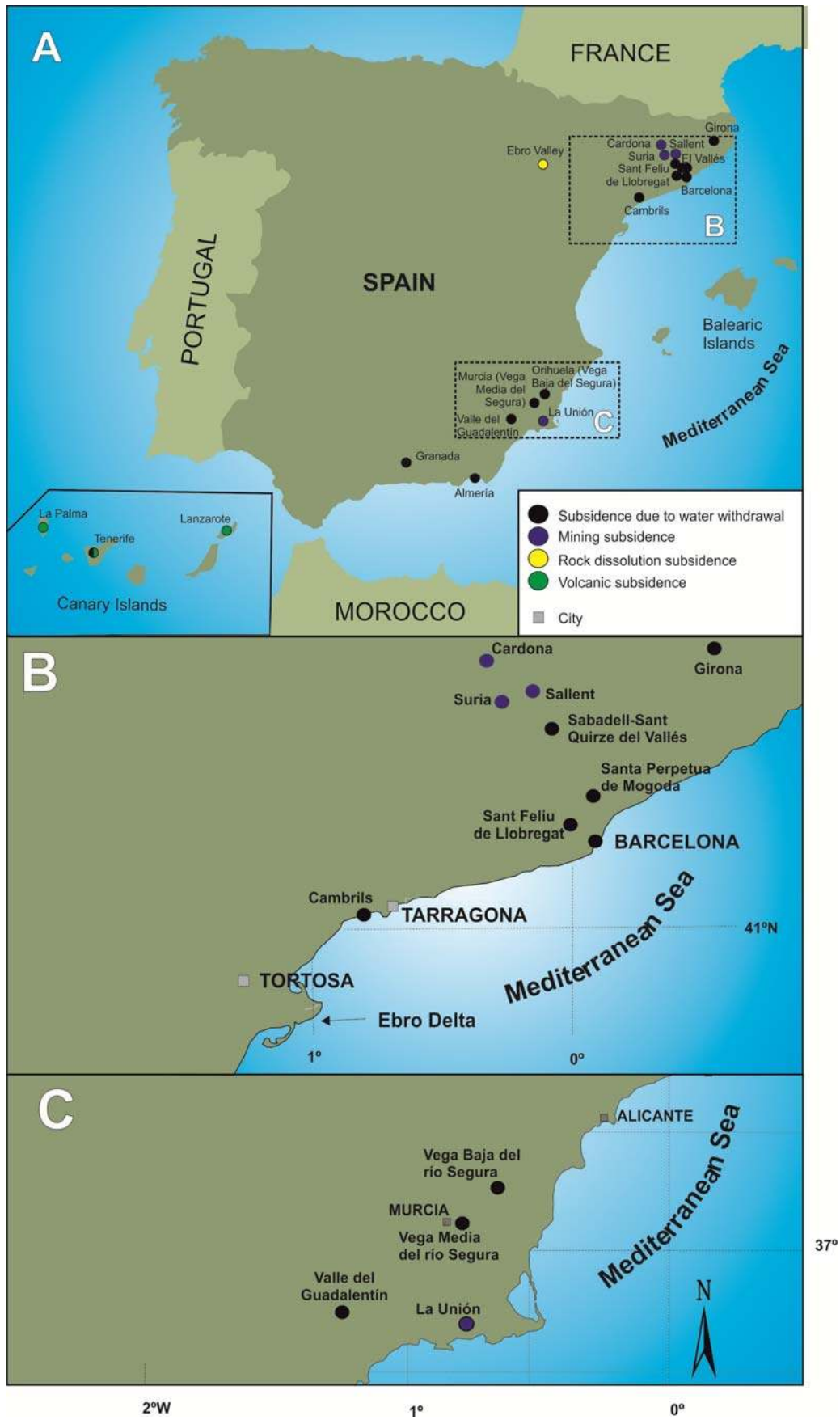


Figure 1



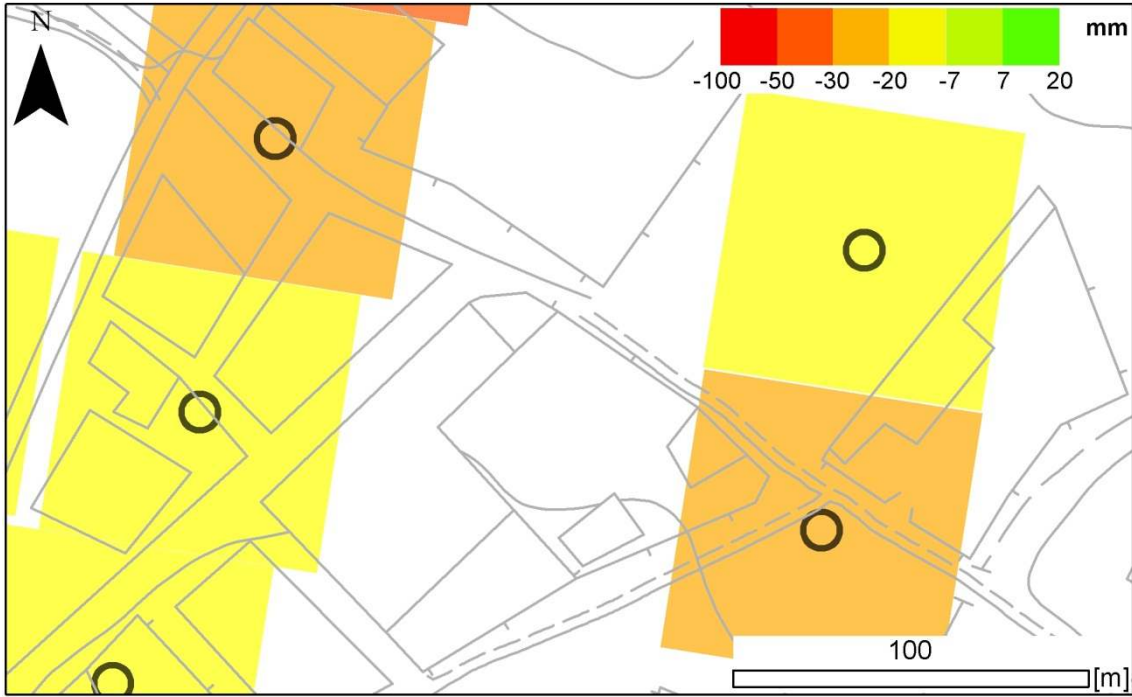


Figure 2

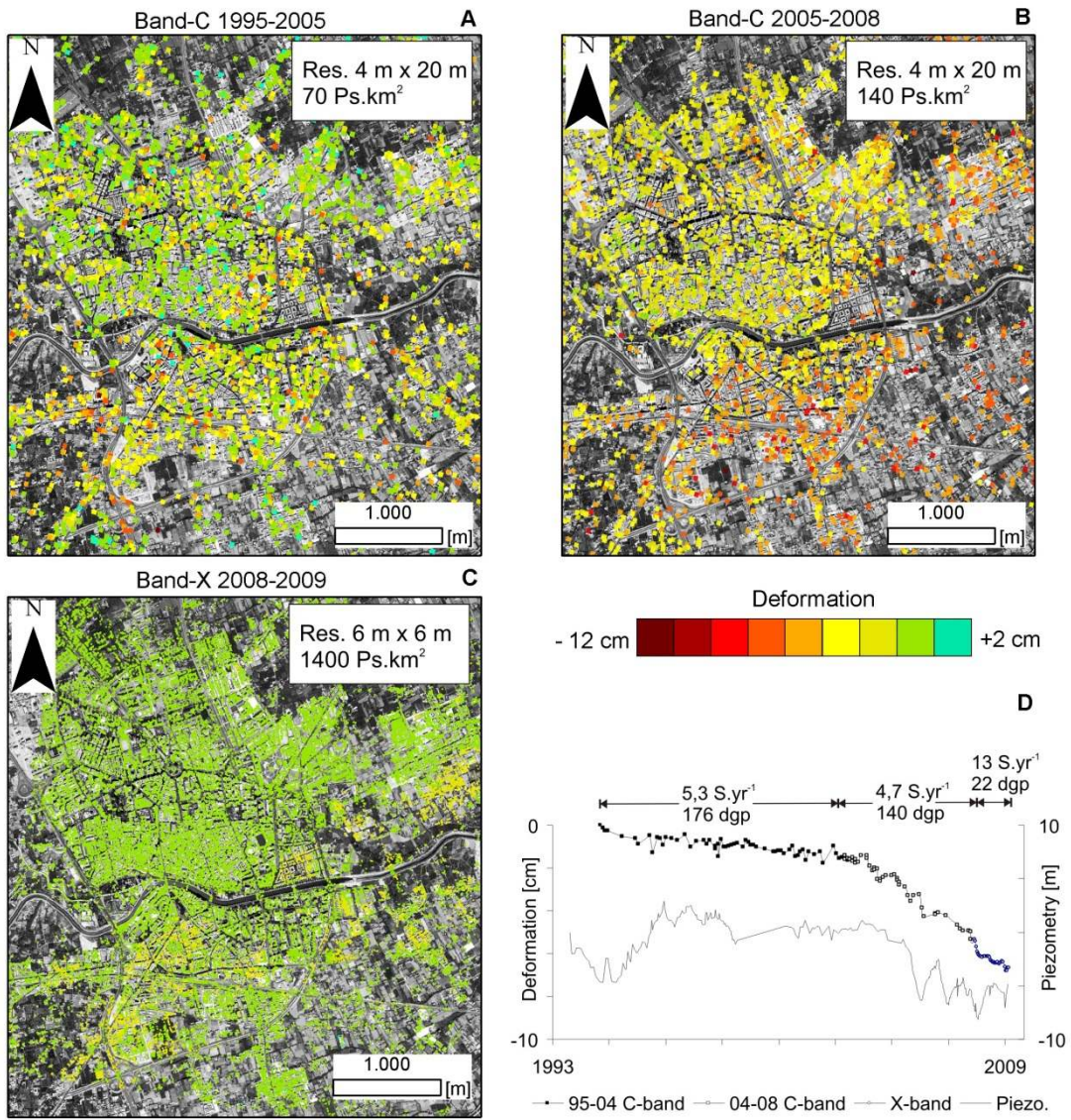


Figure 3



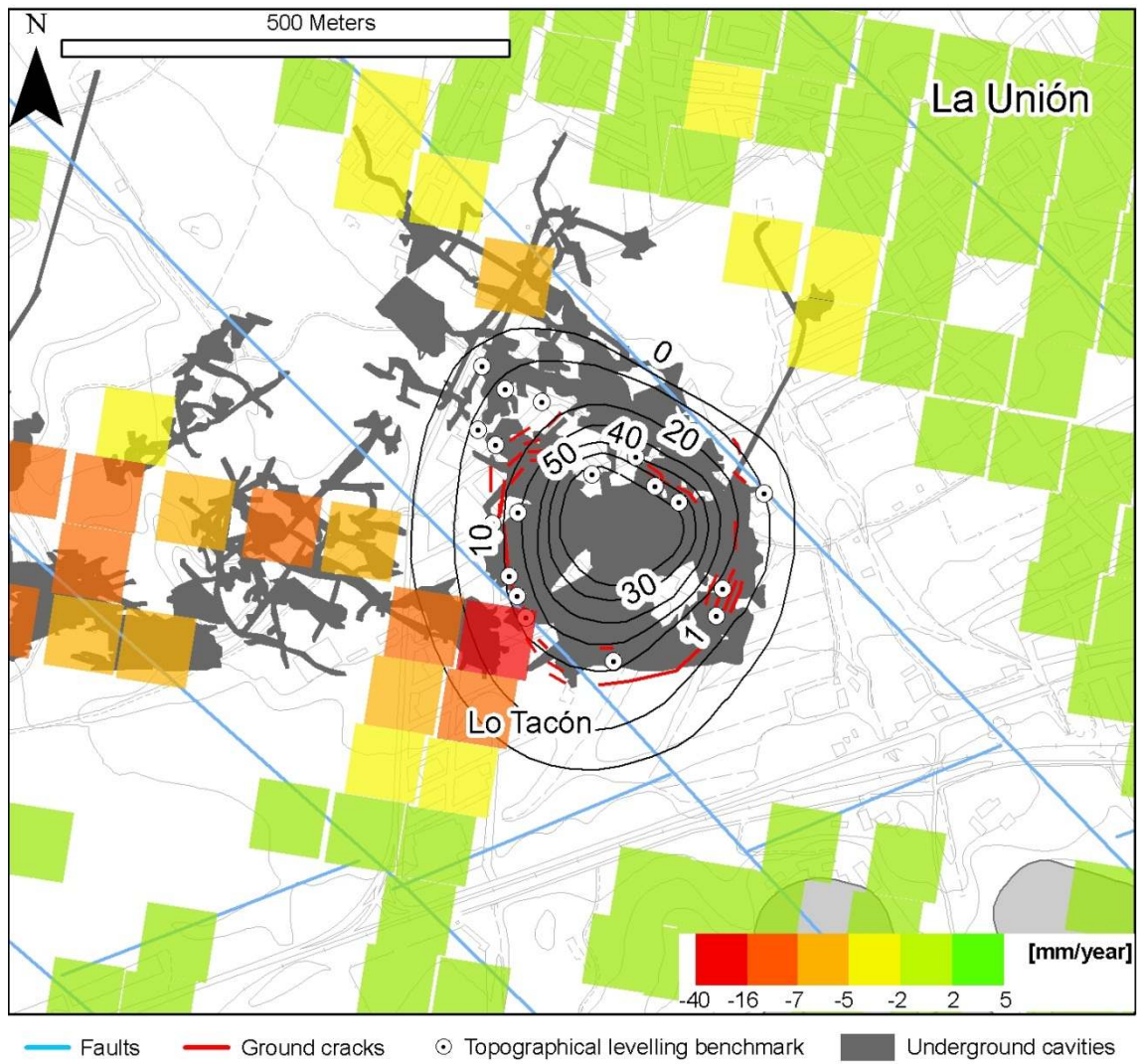


Figure 4

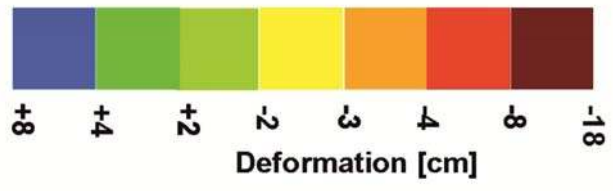


Figure 5

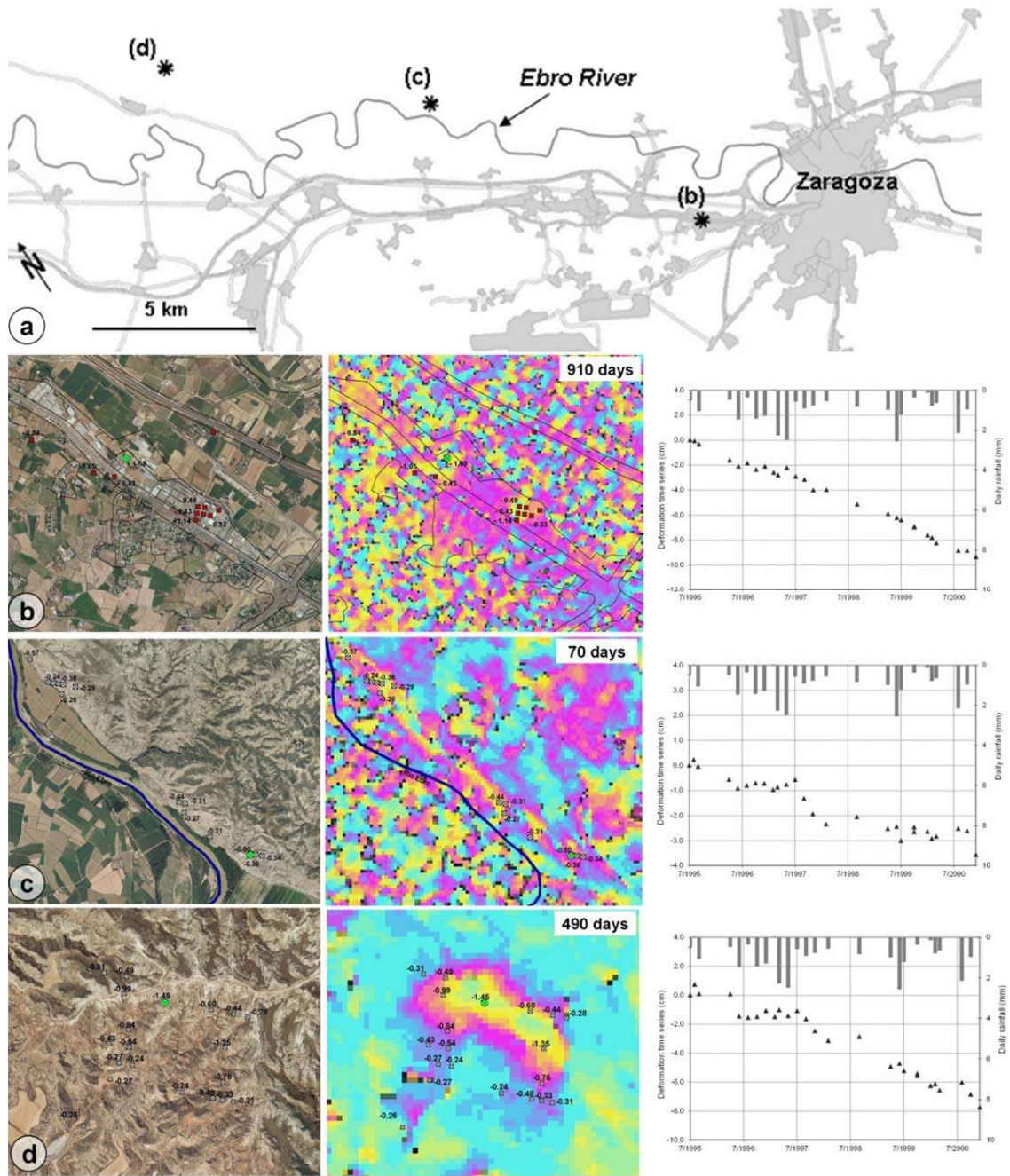


Figure 6

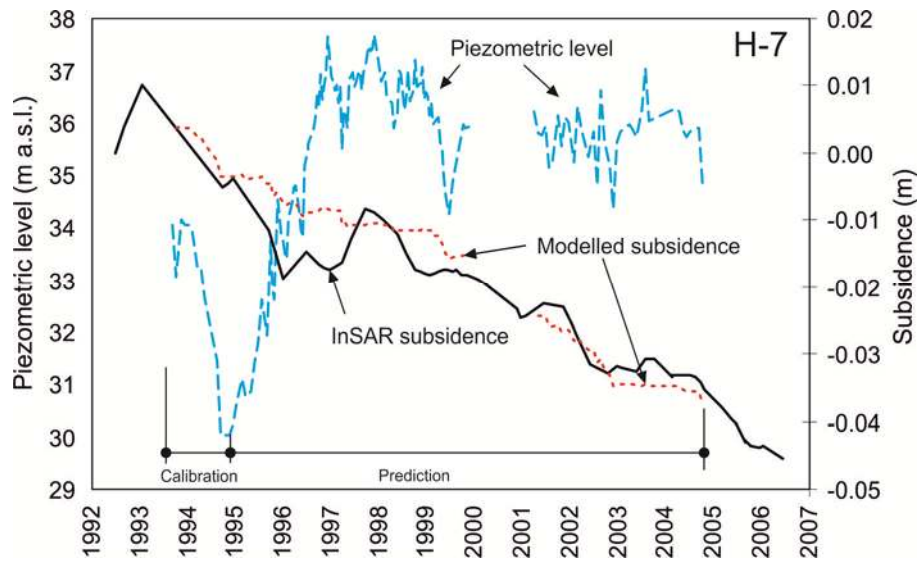


Figure 7

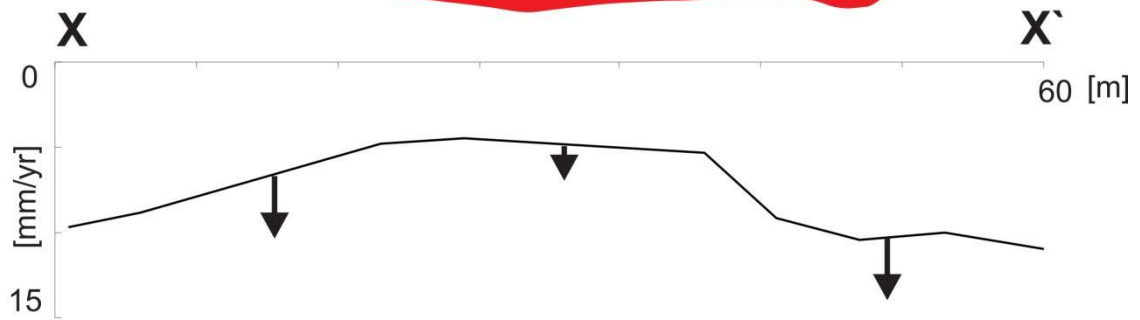
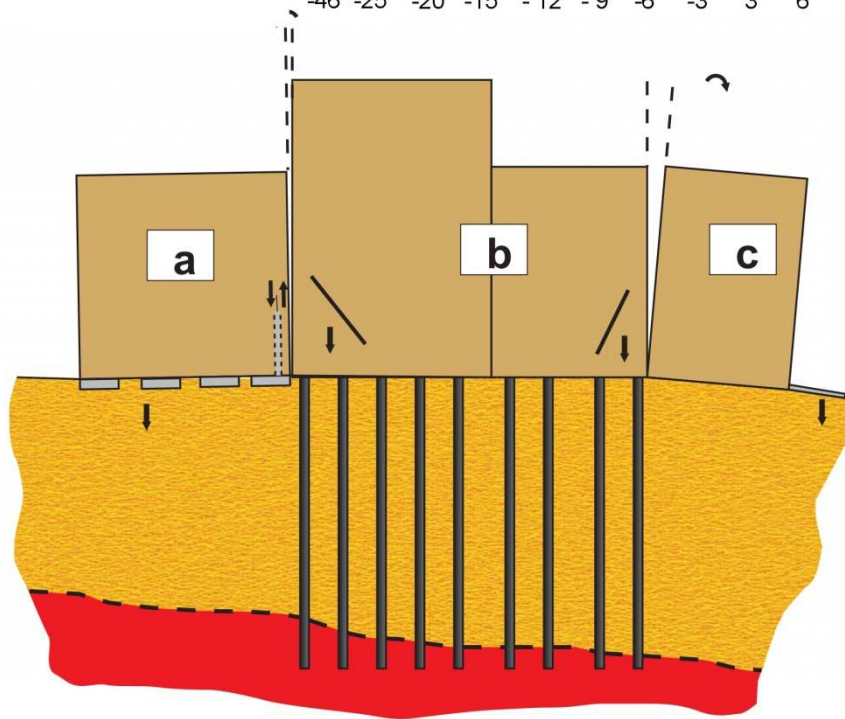
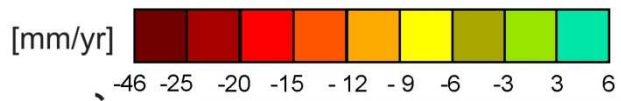
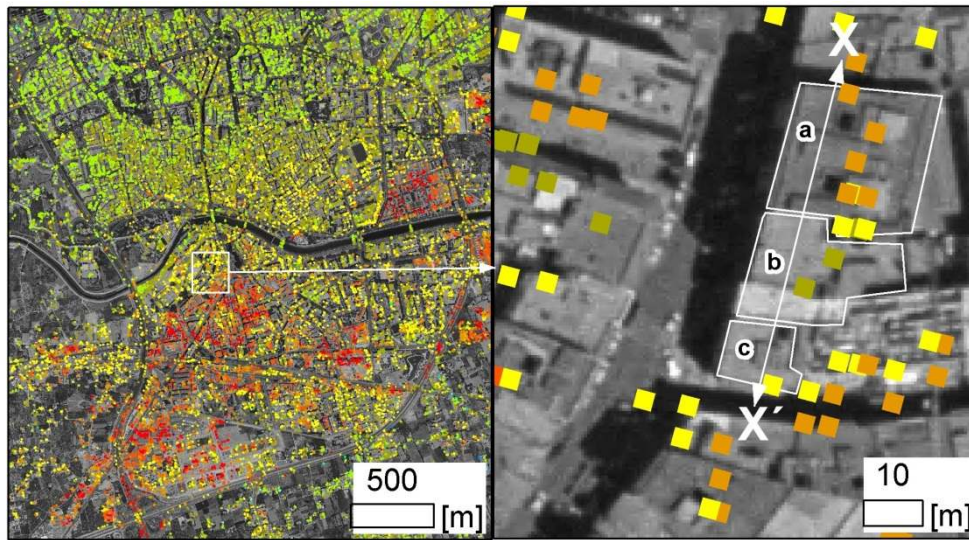


Figure 8



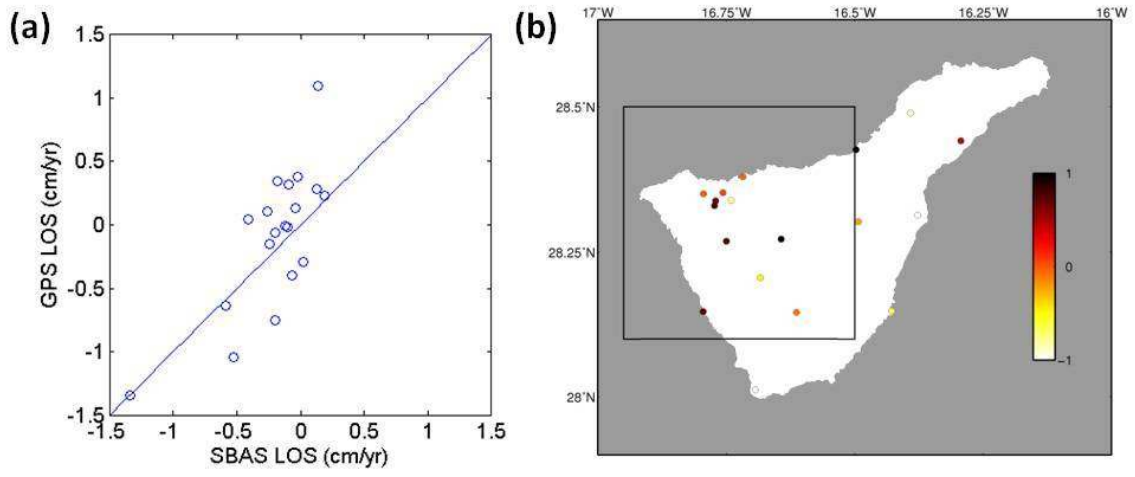


Figure 9

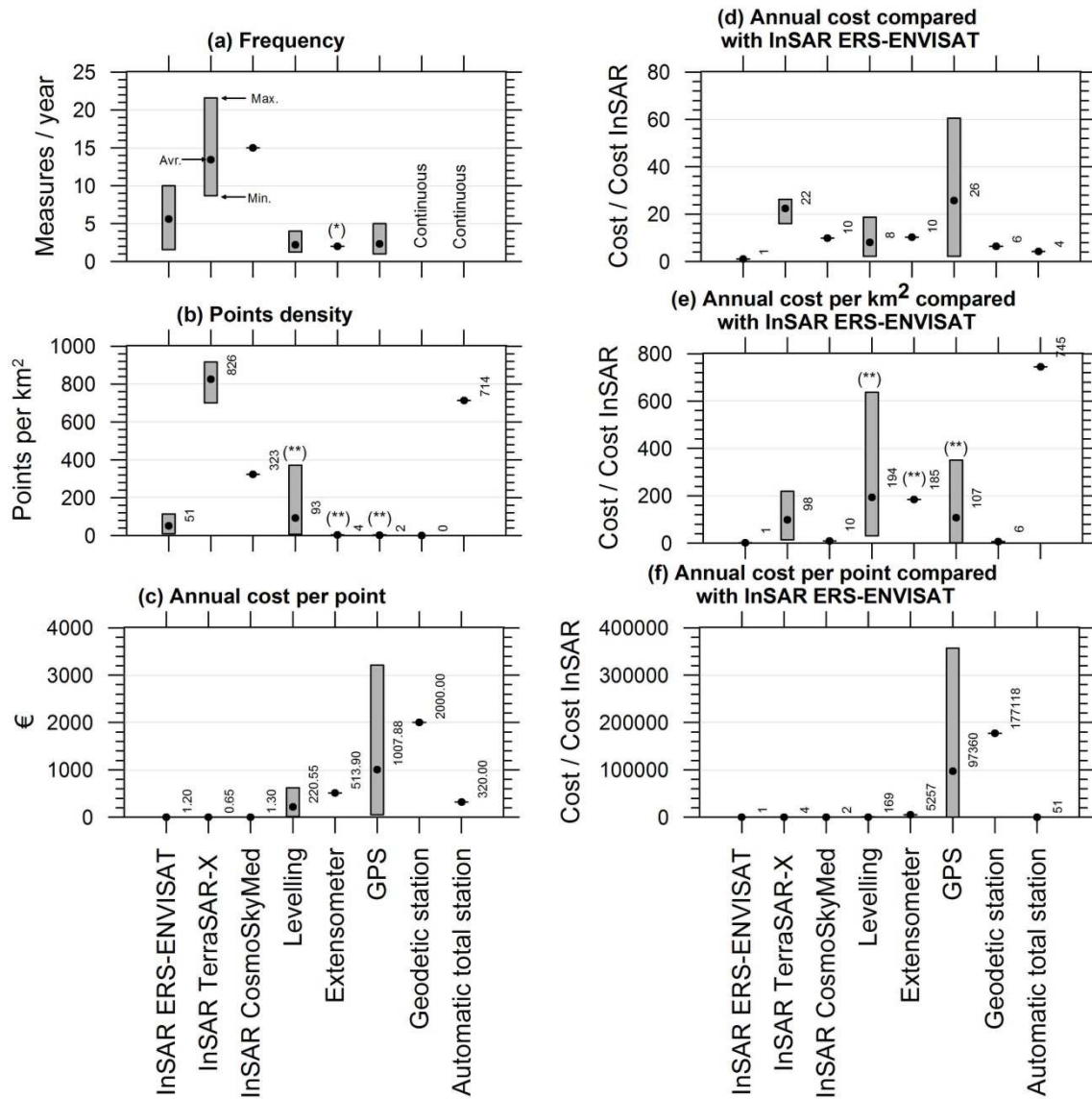


Figure 10